

Reaction of SO₃ with H₂SO₄ and Its Implication for Aerosol Particle Formation in the Gas Phase and at the Air-Water Interface

Rui Wang^a, Yang Cheng^{a,‡}, Shasha Chen^{a,‡}, Rongrong Li^a, Yue Hu^a, Xiaokai Guo^c,
5 Tianlei Zhang^{a,*}, Fengmin Song^a, Hao Li^{b,*}

^a Shaanxi Key Laboratory of Catalysis, School of Chemical & Environment Science, Shaanxi
University of Technology, Hanzhong, Shaanxi 723001, P. R. China

^b State Key Joint Laboratory of Environment Simulation and Pollution Control, Research Center for
Eco-environmental Sciences, Chinese Academy of Sciences, Beijing, 100085, China

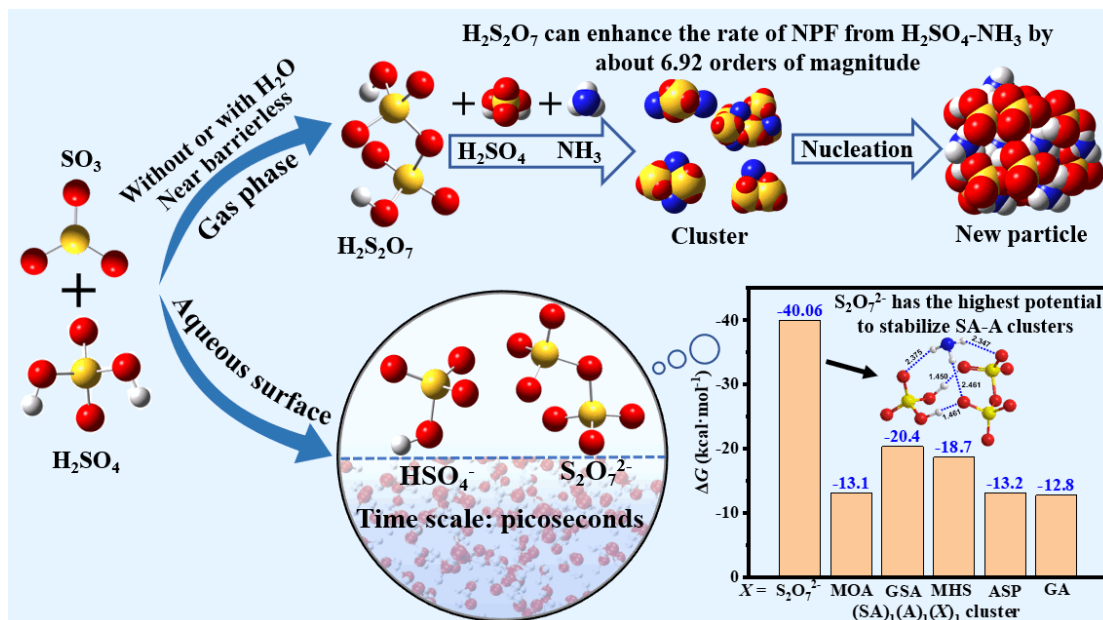
10 ^c Department of Applied Chemistry, Yuncheng University, Yuncheng, Shanxi 044000, China

* Corresponding authors. Tel: +86-0916-2641083, Fax: +86-0916-2641083.

E-mail: ztianlei88@163.com (T. L. Zhang) ; haol@rcees.ac.cn (H. Li)

‡ Yang Cheng and Shasha Chen contributed equally to this work.

Abstract. The reactions between SO_3 and atmospheric acids are indispensable in improving the formation of aerosol particle. However, relative to those of SO_3 with organic acids, the reaction of SO_3 with inorganic acids has not received much attention. Here, we explore the atmospheric reaction between SO_3 and H_2SO_4 , a typical inorganic acid, in the gas phase and at the air-water interface by using quantum chemical (QC) calculations and Born-Oppenheimer molecular dynamics simulations. We also report the effect of $\text{H}_2\text{S}_2\text{O}_7$, the product of the reaction between SO_3 and H_2SO_4 , on new particle formation (NPF) in various environments by using the Atmospheric Cluster Dynamics Code kinetic model and the QC calculation. The present findings show that the gas phase reactions of $\text{SO}_3 + \text{H}_2\text{SO}_4$ without and with water molecule are both low energy barrier processes. With the involvement of interfacial water molecules, H_2O -induced the formation of $\text{S}_2\text{O}_7^{2-} \cdots \text{H}_3\text{O}^+$ ion pair, HSO_4^- mediated the formation of $\text{HSO}_4^- \cdots \text{H}_3\text{O}^+$ ion pair and the deprotonation of $\text{H}_2\text{S}_2\text{O}_7$ were observed and proceeded on the picosecond time-scale. The present findings suggest the potential contribution of SO_3 - H_2SO_4 reaction to NPF and aerosol particle growth as the facts that *i)* although $\text{H}_2\text{S}_2\text{O}_7$ is easily hydrolyzed with water to form H_2SO_4 , it can directly participate in H_2SO_4 - NH_3 -based cluster formation and can present a more obvious enhancement effect on SA-A-based cluster formation; and *ii)* the formed interfacial $\text{S}_2\text{O}_7^{2-}$ can attract candidate species from the gas phase to the water surface, and thus, accelerate particle growth.



Graphic abstract

30 **1 Introduction**

Sulfur trioxide (SO_3) is a major air pollutant (Zhuang and Pavlish, 2012; Chen and Bhattacharya, 2013; Cao et al., 2010; Kikuchi, 2001; Mitsui et al., 2011) and can be considered as the most important oxidation product of SO_2 (Starik et al., 2004). As an active atmospheric species, SO_3 can lead to the formations of acid rain and atmospheric aerosol (Sipilä et al., 2010; Mackenzie et al., 2015; England et al., 2000; Li et al., 2016; Renard et al., 2004) and thus plays a well-35 documented role in regional climate and human health (Zhang et al., 2012; Pöschl, 2005; Zhang et al., 2015; Pöschl and Shiraiwa, 2015; Haywood and Boucher, 2000; Lohmann and Feichter, 2005). In the atmosphere, the hydrolysis of SO_3 to product H_2SO_4 (SA) is the most major loss route of SO_3 (Morokuma and Muguruma, 1994; Akhmatskaya et al., 1997; Larson et al., 2000; Hazra and Sinha, 40 2011; Long et al., 2013a; Torrent-Sucarrat et al., 2012; Ma et al., 2020). As a complement to the loss of SO_3 , ammonolysis reaction of SO_3 in polluted areas of NH_3 can form $\text{H}_2\text{NSO}_3\text{H}$, which not only can be competitive with the formation of SA from the hydrolysis reaction of SO_3 , but also can enhance the formation rates of sulfuric acid (SA)-dimethylamine ($\text{NH}(\text{CH}_3)_2$, DMA) clusters by about 2 times. Similarity, the reactions of SO_3 with CH_3OH and organic acids (such as HCOOH) 45 were reported (Liu et al., 2019; Hazra and Sinha, 2011; Long et al., 2012; Mackenzie et al., 2015; Huff et al., 2017; Smith et al., 2017; Li et al., 2018a), and both processes can provide a mechanism for incorporating organic matter into aerosol particles. However, the reaction mechanism between SO_3 and inorganic species are still unclear.

As a major inorganic acidic air pollutant (Tilgner et al., 2021), SA can act as an important role 50 in the new particle formation (Weber et al., 1995; Weber et al., 1996; Weber et al., 2001; Sihto et al., 2006; Riipinen et al., 2007; Sipilä et al., 2010; Zhang et al., 2012) and acid rain (Calvert et al., 1985; Finlayson-Pitts and Pitts Jr, 1986; Wayne, 2000). The source of gas-phase SA is mainly produced by the gas-phase hydrolysis reaction of SO_3 . For the direct reaction between SO_3 and H_2O , it takes place hardly in the atmosphere due to high energy barrier (Chen and Plummer, 1985; 55 Hofmann and Schleyer, 1994; Morokuma and Muguruma, 1994; Steudel, 1995). However the addition of a second water molecule (Morokuma and Muguruma, 1994; Larson et al., 2000; Loerting and Liedl, 2000), the hydroperoxyl radical (Gonzalez et al., 2010), formic acid (Hazra and Sinha, 2011; Long et al., 2012), sulfuric acid (Torrent-Sucarrat et al., 2012), nitric acid (Long et al., 2013a),

oxalic acid (Lv et al., 2019) and ammonia (Bandyopadhyay et al., 2017) have been reported to catalyze the formation of SA from the hydrolysis reaction of SO_3 as they can promote atmospheric proton transfer reactions. Similarity, as SA can give out protons more readily than H_2O , which in turn is more conducive to the proton transfer, thus we predict that the addition reaction involving the proton transfer between SO_3 and SA is much easier under atmospheric conditions than that between SO_3 and H_2O . However, this gas-phase reaction has not been investigated as far as we know. Previous studies have shown that the concentration of water vapor decreases significantly with increasing altitude (Anglada et al., 2013), leading to longer atmospheric lifetimes of SO_3 . The gas phase reaction of SO_3 with H_2SO_4 may contribute significantly to the loss of SO_3 in dry areas where $[\text{H}_2\text{SO}_4]$ is relatively high (especially at lower temperatures) and at higher altitude. So, it is important to study the reaction mechanism of SO_3 with H_2SO_4 and its competition with H_2O -assisted hydrolysis of SO_3 . Meanwhile, in many gas phase reactions, single water molecule can play a catalyst role by increasing the stability of pre-reactive complexes and reducing the activation energy of transition states (Kanno et al., 2006; Stone and Rowley, 2005; Chen et al., 2014; Viegas and Varandas, 2012, 2016). For example, single water molecule in the $\text{H}_2\text{O}\cdots\text{HO}_2 + \text{SO}_3$ reaction can catalyze the formation of HSO_5 (Gonzalez et al., 2010). Thus, it is equally important to study the $\text{SO}_3 + \text{SA}$ reaction without and with H_2O . In addition to the gas phase reactions, many new atmospheric processes and new reaction pathways have been observed at the air-water interface (Zhong et al., 2017; Kumar et al., 2017; Kumar et al., 2018; Zhu et al., 2016; Li et al., 2016; Zhu et al., 2017). Such as, the organic acids reacting with SO_3 can form the ion pair of carboxylic sulfuric anhydride and hydronium at the air-water interface (Zhong et al., 2019). This mechanism is different from the gas phase reaction in which the organic acid either serves as a catalyst for the hydrolysis of SO_3 or acts as a reactant reacting with SO_3 directly. So, water droplets may play important roles in atmospheric behaviors between SO_3 and SA. Thus, it is also important to study the interfacial mechanism between SO_3 and SA, and to compare its difference with the corresponding gas-phase reaction.

Previous experimental studies (Otto and Steudel, 2001; Abedi and Farrokhpour, 2013) found that disulfuric acid ($\text{H}_2\text{S}_2\text{O}_7$, DSA) is the product of the reaction between SO_3 and SA. From the perspective of structure, DSA possesses two HO functional groups. Both HO groups can act as hydrogen donors and acceptors to interact with atmospheric particle precursors. It has been shown

that the reaction between SO_3 and some important atmospheric species (Li et al., 2018a; Yang et al., 2021; Liu et al., 2019; Rong et al., 2020) not only can cause appreciable consumption of SO_3 and thus reduce the abundance of SA from the hydrolysis of SO_3 in the atmosphere, but also can promote NPF process by their products. For example, the products of $\text{NH}_2\text{SO}_3\text{H}$, $\text{HOOCOOSO}_3\text{H}$, $\text{CH}_3\text{OSO}_3\text{H}$ and $\text{HOCCOOSO}_3\text{H}$ from the reactions of SO_3 with NH_3 (Li et al., 2018a), $\text{H}_2\text{C}_2\text{O}_4$ (Yang et al., 2021), CH_3OH (Liu et al., 2019) and HOOCCHO (Rong et al., 2020) all have a catalytic effect on the formation of new particles in aerosols. However, whether DSA produced by the reaction between SO_3 and SA contributes to aerosol formation or not is still unclear. Thus, another main question that we intend to address here is the role of DSA in atmospheric SA- NH_3 (A) nucleation, which have been recognized as dominant precursors in highly polluted areas, especially in some megacities in Asia.

In this work, using quantum chemical calculations and Master Equation, we first studied the gas-phase reaction between SO_3 and SA to product DSA with H_2O acting as a catalyst. Then, we use the Born-Oppenheimer Molecular Dynamic (BOMD) simulations to evaluate the reaction mechanism of SO_3 with SA at the air-water interface. Finally, we used Atmospheric Clusters Dynamic Code (ACDC) and quantum chemical calculations to investigate atmospheric implications of SO_3 -SA reaction to the atmospheric particle formation. Particular attention of this work is focused on the study of *i*) the mechanism difference of the $\text{SO}_3 + \text{SA}$ reaction in the gas phase and at the air-water interface; *ii*) the fate of DSA in atmospheric NPF and its influence at various environmental conditions.

2 Computational details

2.1 Quantum chemical calculation. The M06-2X functional has been proved to be one of the best functionals to describe the noncovalent interactions and estimate the thermochemistry and equilibrium structures for atmospheric reactions (Elm et al., 2012; Mardirossian and Head-Gordon, 2016). So, for the $\text{SO}_3 + \text{SA}$ reaction without and with water molecule in the gas phase, the optimized geometries and vibrational frequencies of reactants, pre-reactive complexes, transition states (TSS), post-reactive complexes and products were calculated using M06-2X method (Zhao and Truhlar, 2008; Elm et al., 2012) with 6-311++G(2df,2pd) basis set by Gaussian 09 packages (Frisch, 2009). It is noted that the calculated

bond distances and bond angles at the M06-2X/6-311++G(3df,2pd) level (Figure S1) agree well with the available experimental values (Kuczkowski et al., 1981). At the same level, the connectivity
120 between the TSs and the suitable pre- and post-reactant complexes was performed by intrinsic reaction coordinate (IRC) calculations. Then, single point energy calculations were calculated at the CCSD(T)-F12/cc-pVDZ-F12 level (Adler et al., 2007; Knizia et al., 2009) by using ORCA (Neese, 2012).

A multistep global minimum sampling technique was used to search for the global minima of
125 the (DSA)_x(SA)_y(A)_z ($z \leq x + y \leq 3$) molecular clusters. Specifically, a multistep global minimum sampling technique was used to search for the global minima of the (SA)_x(A)_y(DSA)_z ($0 < y \leq x + z \leq 3$) clusters. Specifically, the initial $n \times 1000$ ($1 < n < 5$) configurations for each cluster were systematically generated by the ABCcluster program (Zhang and Dolg, 2015), and were optimized at the semi-empirical PM6 (Stewart, 2013) methods using MOPAC 2016 (Stewart, 2013; Stewart,
130 2007). Then, up to $n \times 100$ structures with relatively lowest energy among the $n \times 1000$ ($1 < n < 5$) structures were selected and reoptimized at the M06-2X/6-31+G(d,p) level. Finally, $n \times 10$ lowest-lying structures were optimized by the M06-2X/6-311++G(2df,2pd) level to determine the global minimum. To obtain the reliable energies, single-point energy calculations were refined at the DLPNO-CCSD(T)/aug-cc-pVTZ level based on the optimized geometries at the M06-2X/6-
135 311++G(2df,2pd) level. The optimized structures and the formation Gibbs free energy of the stable clusters were summarized in Figure S9 and Table S8 of the *SI Appendix*, respectively.

2.2 Rate constant calculations. Using the Rice-Ramsperger-Kassel-Marcus based Master Equation (ME/RRKM) model (Miller and Klippenstein, 2006), the kinetics for the SO₃ + SA reaction without and with water molecule were calculated by adopting a Master Equation Solver
140 for Multi Energy-well Reactions (MESMER) code (Glowacki et al., 2012). In the MESMER calculation, the rate coefficients for the bimolecular barrierless association step (from reactants to pre-reactive complexes) were evaluated by the Inverse Laplace Transform (ILT) method (Horváth et al., 2020), meanwhile the unimolecular step was performed by the RRKM theory combined with the asymmetric Eckart model. The ILT method and RRKM theory can be represented in Eq (1) and
145 Eq (2), respectively.

$$k^\infty(\beta) = \frac{1}{Q(\beta)} \int_0^\infty k(E) \rho(E) \exp(-\beta E) dE \quad (1)$$

$$k(E) = \frac{W(E - E_0)}{h\rho(E)} \quad (2)$$

Where h is denoted as Planck's constant; $\rho(E)$ is denoted as the active density of state of the reactant at energy level E ; E_0 is denoted as the reaction threshold energy and $W(E-E_0)$ is denoted as the sum of the rovibrational states of the transition state (TS) geometry (excluding the degree of freedom related to passing the transition state). The input parameters for electronic geometries, vibrational frequencies, and rotational constants were calculated at the M06-2X/6-311++G(2df,2pd) level and single-point energy calculations were refined at the CCSD(T)-F12/cc-pVDZ-F12 level for the modeling.

2.3 Born-Oppenheimer Molecular Dynamic (BOMD) simulation. The CP2K code (Hutter et al., 2014) was used in the BOMD simulations. The Becke-Lee-Yang-Parr (BLYP) functional (Becke, 1988; Lee et al., 1988) was chosen to treat with the exchange and correlation interactions, and the Grimme's dispersion was carried out to account for the weak dispersion interaction (Grimme et al., 2010). The Goedecker-Teter-Hutter (GTH) conservation pseudopotential (Goedecker et al., 1996; Hartwigsen et al., 1998) with the Gaussian DZVP basis set (VandeVondele and Hutter, 2007) and the auxiliary plane wave basis set was applied to correct the system valence electrons and the core electrons, respectively. For the plane wave basis set and Gaussian basis set, the energy cut off (Zhong et al., 2017; Zhong et al., 2018; Zhong et al., 2019) were set to 280 and 40 Ry, respectively. For each simulation in the gas phase, a $15 \times 15 \times 15 \text{ \AA}^3$ supercell with periodic boundary condition was adopted with a time step of 0.5 fs. As the droplet system with 191 water molecules are sufficient to describe the interfacial mechanism (Zhong et al., 2017), the air-water interfacial system here included 191 water molecules, SO_3 and SA in the BOMD simulation. It is pointed out that the droplet system with 191 water molecules has been equilibrated before SO_3 and H_2SO_4 was added at the water surface. The details of the equilibrium process for the droplet system with 191 water molecules are shown in the *SI Appendix* Part 4. To avoid periodic interactions between adjacent water droplets, the size of the simulation box (Kumar et al., 2017; Kumar et al., 2018; Ma et al., 2020) was set as $35 \times 35 \times 35 \text{ \AA}^3$ with a time step of 1.0 fs. Notably, the timestep of 1.0 fs has been proved to achieve sufficient energy conservation for the water system (Zhong et al., 2015; Li et al., 2016; Zhu et al., 2016; Kumar et al., 2017). For all the simulations in the gas phase and at the air-water

interface, the Nose-Hoover thermostat (Zhong et al., 2017; Zhong et al., 2018; Zhong et al., 2019; Kumar et al., 2017; Kumar et al., 2018; Ma et al., 2020) was selected the NVT ensemble to control the temperature around 300 K. To eliminate the influence of the initial configuration on the simulation results of interfacial reaction, 40 BOMD simulations for the air-water interface reactions were carried out.

2.4 Atmospheric Clusters Dynamic Code (ACDC) model

The Atmospheric Cluster Dynamics Code (ACDC) (McGrath et al., 2012) was used to simulate the cluster formation rates and mechanisms of $(\text{DSA})_x(\text{SA})_y(\text{A})_z$ ($z \leq x + y \leq 3$) clusters at different temperatures and monomer concentrations. The thermodynamic data of quantum chemical calculation at the DLPNO-CCSD(T)/aug-cc-pVTZ//M06-2X/6-311++G(2df,2pd) level of theory can be used as the input of ACDC. The birth-death equation (Eq. 3) for clusters solves the time development of cluster concentrations by numerical integration using the ode15s solver in MATLAB program (Shampine and Reichelt, 1997).

$$\frac{dc_i}{dt} = \frac{1}{2} \sum_{j < i} \beta_{j,(i-j)} C_j C_{(i-j)} + \sum_j \gamma_{(i+j) \rightarrow i} C_{i+j} - \sum_j \beta_{i,j} C_i C_j - \frac{1}{2} \sum_{j < i} \gamma_{i \rightarrow j} C_i + Q_i - S_i \quad (3)$$

Where c_i is the concentration of cluster i ; β_{ij} is the collision coefficient between clusters i and j ; $\gamma_{(i+j) \rightarrow i}$ is the evaporation coefficient of cluster $i+j$ evaporating into clusters i and j , and Q_i is all other source term of cluster i . (See more details of β and γ in *SI Appendix* Part 4). Besides, a constant coagulation sink coefficient $2 \times 10^{-2} \text{ s}^{-1}$ (corresponding to the median observed in contaminated areas) was used for taking into account external losses (Yao et al., 2018; Zhang et al., 2022; Liu et al., 2021b). The boundary conditions in the ACDC require that the smallest clusters outside of the simulated system should be very stable so that not to evaporate back immediately (McGrath et al., 2012). Based on cluster volatilization rate (shown in Table S10) and the formation Gibbs free energy of the clusters (shown in Table S8), the cluster boundary conditions simulated in this study were set as $(\text{SA})_4 \cdot (\text{A})_3$, $(\text{SA})_4 \cdot (\text{A})_4$, $\text{SA} \cdot (\text{A})_3 \cdot (\text{DSA})_3$, $(\text{SA})_3 \cdot (\text{A})_4 \cdot (\text{DSA})_1$ and $(\text{SA})_2 \cdot (\text{A})_3 \cdot (\text{DSA})_2$. According to field observations, the concentration of SA and A was respectively set in a range of 10^6 - $10^8 \text{ molecules} \cdot \text{cm}^{-3}$ and 10^7 - $10^{11} \text{ molecules} \cdot \text{cm}^{-3}$ (Almeida et al., 2013; Kuang et al., 2008; Bouo et al., 2011; Zhang et al., 2018). As the prediction in Table S7, the concentration of DSA is set to 10^4 - $10^8 \text{ molecules} \cdot \text{cm}^{-3}$. However, DSA is easily hydrolyzed with abundant water in the troposphere to form H_2SO_4 , the concentration of DSA listed in Figure S9 was overestimated.

205 So, the maximum concentration of DSA (10^8 molecules·cm⁻³) was not included in the effect of H₂S₂O₇ on new particle formation (NPF) in various environments. Besides, the temperature was set to be 218.15-298.15 K, which span most regions of the troposphere and the polluted atmospheric boundary layer.

3 Results and discussion

210 3.1 Reactions in the gas phase

The addition reaction involving the proton transfer between SO₃ and SA (Channel DSA) proceeded through the formation of SO₃···H₂SO₄ complex followed by unimolecular transformation through transition state TS_{DSA} to form H₂S₂O₇ (Figure 1(a)). The reactant complex SO₃···H₂SO₄ was a double six-membered ring complex with a relative Gibbs free energy of -1.6 kcal·mol⁻¹. After 215 the formation of SO₃···H₂SO₄ complex, Channel DSA overcame a Gibbs free energy barrier of 2.3 kcal·mol⁻¹, which was lower by 4.2 kcal·mol⁻¹ than that of H₂O-catalyzed hydrolysis of SO₃ (Figure S1). Rate constant for the SO₃ + SA reaction was calculated at various temperatures (Table 1). Within the temperature range of 280-320 K, the rate constants for the SO₃ + SA reaction were calculated to be 2.57×10^{-12} - 5.52×10^{-12} cm³·molecule⁻¹·s⁻¹, which were larger by 3.43-4.03 times 220 than the corresponding values of H₂O-catalyzed hydrolysis of SO₃. Therefore, it can be said that the direct reaction between SO₃ and SA occurs easily under atmospheric conditions.

The SO₃ + H₂SO₄ reaction with H₂O produced two distinct products, labeled (i) H₂S₂O₇ (DSA, Channel DSA_WM) and (ii) H₂SO₄ (SA, Channel SA_SA). A single water molecule in (i) acted as a catalyst, while it played as a reactant in (ii). The schematic potential energy surface for the SO₃ + 225 H₂SO₄ reaction with H₂O was shown in Figure 1. As the probability of simultaneous collision (Pérez-Ríos et al., 2014; Elm et al., 2013) of three molecules of SO₃, SA and H₂O was quite low under realistic conditions, both Channel DSA_WM and Channel SA_SA can be considered as a sequential bimolecular process. In other words, both Channel DSA_WM and Channel SA_SA occurred via the collision between SO₃ (or H₂SO₄) and H₂O to form dimer (SO₃···H₂O and 230 H₂SO₄···H₂O) first, and then the dimer encountered with the third reactant H₂SO₄ or SO₃. The computed Gibbs free energies of dimer complexes SO₃···H₂O and H₂SO₄···H₂O were respectively 0.8 kcal·mol⁻¹ and -1.9 kcal·mol⁻¹, which were respectively consistent with the previous values (the range from -0.2 to 0.62 kcal·mol⁻¹ for SO₃···H₂O complex (Bandyopadhyay et al., 2017; Long et

al., 2012) and the range from -1.82 to -2.63 kcal·mol⁻¹ for H₂SO₄···H₂O complex (Long et al., 2013b;
235 Tan et al., 2018)). The Gibbs free energy of H₂SO₄···H₂O was lower by 2.7 kcal·mol⁻¹ than that of
SO₃···H₂O, thus leading to that the equilibrium constant of the former complex was larger by 1-2
orders of magnitude than that of the latter one in Table S2. Additionally, the larger equilibrium
constant of H₂SO₄···H₂O complex led to its higher concentration in the atmosphere. For example,
when the concentrations of SO₃ (Yao et al., 2020), H₂SO₄ (Liu et al., 2015) and H₂O (Anglada et al.,
240 2013) were 10⁶, 10⁸ and 10¹⁷ molecules·cm⁻³, respectively, the concentrations of SO₃···H₂O and
H₂SO₄···H₂O were 2.41 × 10³-2.01 × 10⁴ and 5.01 × 10⁵-3.01 × 10⁸ molecules·cm⁻³ within the
temperature range of 280-320 K (see Table S3), respectively. So, we predict that Channel DSA_WM
and Channel SA_SA mainly take place via the collision of H₂SO₄···H₂O with SO₃. In order to check
this prediction, the effective rate constants for two bimolecular reactions of H₂SO₄···H₂O + SO₃ and
245 SO₃···H₂O + H₂SO₄ were calculated, and the details were shown in *SI Appendix*, Part 3 and Table
1. As seen in Table 1, the SO₃···H₂O + H₂SO₄ reaction in both Channel DSA_WM and Channel
SA_SA can be neglected as their effective rate constants were smaller by 16.7-48.5 and 1.02-3.05
times than the corresponding values in the H₂SO₄···H₂O + SO₃ reaction within the temperature range
of 280-320 K, respectively. Therefore, we only considered the H₂SO₄···H₂O + SO₃ bimolecular
250 reaction in both Channel DSA_WM and Channel SA_SA.

As for Channel DSA_WM, the H₂SO₄···H₂O + SO₃ reaction occurred in a stepwise process as
displayed in Figure 1(b), which was similar to the favorable routes in the hydrolysis of COS, HCHO
and CH₃CHO catalyzed by sulfuric acid (Long et al., 2013b; Li et al., 2018b; Tan et al., 2018). When
the H₂SO₄···H₂O complex and SO₃ served as reactants, the reaction was initiated by complex
255 IM_{DSA_WM}' where a van der Waals interaction (S2···O4, 2.75 Å) was found between the O4 atom of
SA moiety in H₂SO₄···H₂O and the S atom of SO₃. After complex IM_{DSA_WM}', the ring enlargement
from IM_{DSA_WM}' to SO₃···H₂SO₄···H₂O complex occurred through transition state TS_{DSA_WM}' with
a Gibbs free energy barrier of 1.2 kcal·mol⁻¹. Complex IM_{DSA_WM} was 6.1 kcal·mol⁻¹ lower in energy
than IM_{DSA_WM}'. In IM_{DSA_WM}, SO₃ acted as double donors of hydrogen bond to form a cage-like
260 hydrogen bonding network with H₂SO₄···H₂O. Then, starting with IM_{DSA_WM} complex, the
H₂SO₄···H₂O + SO₃ reaction occurred through transition state TS_{DSA_WM} with a Gibbs free barrier
energy of 0.5 kcal·mol⁻¹ to form a quasi-planar network complex, H₂S₂O₇···H₂O. TS_{DSA_WM} was in
the middle of a double proton transfer, where H₂O played as a bridge for proton transfer, along with

the simultaneous formation of the O4...S2 bond. In order to estimate the catalytic ability of H₂O in the SO₃ + SA reaction, the effective rate constant ($k'_{\text{DSA_WM}_s}$) of the H₂SO₄...H₂O + SO₃ reaction were compared with the rate constant (k_{DSA}) of the SO₃ + H₂SO₄ reaction. As seen in Table 1, under the experimental concentration (Anglada et al., 2013) ([H₂O] = 5.20 × 10¹⁶-2.30 × 10¹⁸ molecules·cm⁻³) within the temperature range of 280-320 K, the calculated $k'_{\text{DSA_WM}_s}$ was 1.03 × 10⁻¹¹-4.60 × 10⁻¹² cm³·molecule⁻¹·s⁻¹, which was larger by 1.79-1.86 times than that of k_{DSA} . This result shows that H₂O exerts catalytic role in promoting the rate of the SO₃ + H₂SO₄ reaction.

Regarding Channel SA_SA, the stepwise reaction occurred firstly via the ring enlargement from six-membered ring complex IM_{SA_SA}' to a cage-like hydrogen bonding network IM_{SA_SA}, and then took place by going through a transition state, TS_{SA_SA}, to form the product complex (H₂SO₄)₂. TS_{DSA_WM} was in the middle of a double hydrogen transfer, where H₂SO₄ acted as a bridge of hydrogen atom from the H₂O to SO₃ along with O1 atom of H₂O addition to the S atom of SO₃. It was worth noting that the energy barriers of two elementary reactions involved in the stepwise route of Channel SA_SA were only 1.8 and 0.6 kcal·mol⁻¹, respectively, showing that the stepwise route of Channel SA_SA is feasible to take place from energetic point of view. To check whether Channel DSA_WM is more favorable than Channel SA_SA or not, their rate ratio listed in Eq. 4 has been calculated in Table 1. The calculated rate ratio $\frac{v_{\text{DSA_WM}}}{v_{\text{SA_SA}}}$ shows that Channel DSA_WM is more important than Channel SA_SA because the rate ratio $\frac{v_{\text{DSA_WM}}}{v_{\text{SA_SA}}}$ is 1.53-3.04 within the temperature range of 280-320 K. So, we predicted that the SO₃ + H₂SO₄ reaction with H₂O producing H₂S₂O₇ is more favorable than that forming H₂SO₄.

$$\frac{v_{\text{DSA_WM}}}{v_{\text{SA_SA}}} = \frac{v_{\text{DSA_WM}_s} + v_{\text{DSA_WM}_o}}{v_{\text{SA_SA}_s} + v_{\text{SA_SA}_o}} = \frac{k_{\text{DSA_WM}_s} \times K_{\text{eq}(\text{H}_2\text{SO}_4 \cdots \text{H}_2\text{O})} + k_{\text{DSA_WM}_o} \times K_{\text{eq}(\text{SO}_3 \cdots \text{H}_2\text{O})}}{k_{\text{SA_SA}_s} \times K_{\text{eq}(\text{H}_2\text{SO}_4 \cdots \text{H}_2\text{O})} + k_{\text{SA_SA}_o} \times K_{\text{eq}(\text{SO}_3 \cdots \text{H}_2\text{O})}} \quad (4)$$

3.2 Reactions at the air-water interface

The mechanism for the SO₃ + SA reaction at the air-water interface was lacking. Notably, SO₃, SA and DSA molecules can stay at the interface for 35.8%, 30.1% and 39.2% of the time in the 150 ns simulation (Figure S2), respectively, revealing that the existence of SO₃, SA and DSA at the air-water interface cannot be negligible. So, the BOMD simulations were used to evaluate the reaction mechanism of SO₃ with SA at the aqueous interfaces. Similar with the interfacial reaction of SO₃ with organic and inorganic acids (Cheng et al., 2023; Zhong et al., 2019), the reaction between SO₃

and SA at the aqueous interface may occur in three ways: (i) SO₃ colliding with adsorbed SA at the air-water interface; (ii) SA colliding with adsorbed SO₃ at the aqueous interface; or (iii) the SO₃-SA complex reacting at the aqueous interface. However, due to the high reactivity both of SO₃ and SA at the air-water interface, the lifetimes of SO₃ (Zhong et al., 2019) and SA (Figure S3) (on the order of a few picoseconds) on the water droplet were extremely short and can be formed SA⁻ ion quickly. Besides, as the calculated result above, SO₃⋯H₂SO₄ complex can be generate DSA easily before it approaches the air-water interface. So, two possible models were mainly considered for the SO₃ + SA reaction on the water surface: (i) gaseous SO₃ colliding with SA⁻ at the air-water interface and (ii) the DSA (the gas-phase product of SO₃ and SA) dissociating on water droplet.

Gaseous SO₃ colliding with SA⁻ at the air-water interface. At the water droplet's surface, the interaction between SO₃ and SA⁻ included two main channels: (i) H₂O-induced formation of S₂O₇²⁻⋯H₃O⁺ ion pair (Figure 2, Figure S4 and Movie S1) and (ii) SA⁻-mediated formation of SA⁻⋯H₃O⁺ ion pair (Figure 3, Figs. S5-S6 and Movies S2-S3). The BOMD simulations for H₂O-induced formation of S₂O₇²⁻⋯H₃O⁺ ion pair was illustrated in Figure 2, the H1 atom of SA⁻ ion can combine with a nearby interfacial water molecule at 8.18 ps by hydrogen bond ($d_{(O3-H1)} = 1.17 \text{ \AA}$) interaction, thus forming hydrated hydrogen sulfate ion (SA⁻⋯H₂O). Then, the H1 atom of SA⁻ ion was moved to the O3 atom of the interfacial water molecule at 8.28 ps, revealing the formation of SO₄²⁻⋯H₃O⁺ ion pair. Additionally, SO₄²⁻ gradually approached to SO₃ molecule with the shortening of S1-O1 bond. At 9.26 ps, the S1-O1 bond length was 1.84 Å, which was close to the length of S-O1 (1.65 Å) bond in S₂O₇²⁻ ion (Figure S8), revealing the formation of S₂O₇²⁻⋯H₃O⁺ ion pair.

Both direct (Figure 3(a), Figure S5 and Movie S2) and indirect (Figure 3(b), Figure S6 and Movie S3) forming mechanisms were observed in SA⁻-mediated formation of SA⁻⋯H₃O⁺ ion pair. The direct SA⁻-mediated formation of SA⁻⋯H₃O⁺ ion pair was a loop structure mechanism, which was consistent with gas phase hydrolysis of SO₃ assisted by acidic catalysts of HCOOH, HNO₃, H₂C₂O₄ and SA in the previous works (Long et al., 2012; Long et al., 2013a; Torrent-Sucarrat et al., 2012; Lv et al., 2019), and the interfacial reactions of HNO₃-mediated Criegee hydration (Kumar et al., 2018) and the hydration of SO₃ via the loop-structure formation (Lv and Sun, 2020). As for the direct formation mechanism of SA⁻⋯H₃O⁺ ion pair seen in Figure 3(a) and movie S2, an eight-membered loop complex, SO₃⋯H₂O(1)⋯SA⁻, was found at 1.46 ps with the formations of two hydrogen bonds ($d_{(O3\cdots H2)} = 2.13 \text{ \AA}$; $d_{(O4\cdots H3)} = 2.18 \text{ \AA}$) and a van der Waals interaction ($d_{(S1\cdots O1)} =$

2.14 Å). Subsequently, SO₃ and interfacial H₂O(1) were close to each other. At 1.59 ps, a transition state-like loop structure was observed and proton transfer from interfacial H₂O(1) to another suspended H₂O(2) was found, where the bond lengths of S1-O1, O1-H1 and H1-O2 were 1.94 Å, 1.19 Å and 1.32 Å, respectively. At 1.70 ps, the bond lengths of S-O1 and H1-O2 were reduced to 1.73 Å and 1.01 Å, while the bond length of H1-O2 was extended to 1.61 Å, showing the formation of SA⁻···H₃O⁺ ion pair. During the direct formation route of SA⁻···H₃O⁺ ion pair, SA⁻ played as a spectator, while interfacial water molecules acted as both a reactant and a proton acceptor. As compared with the hydration reaction mechanism of SO₃ at the air-water interface reported by Lv et al. (Lv and Sun, 2020), the loop-structure formation with proton transferred in the loop was not observed in the direct mechanism of SA⁻-mediated formation of SA⁻···H₃O⁺ ion pair. This was probably because SA⁻ ion was more difficult to give the proton.

As seen in Figure 3(b) and Movie S3, the indirect forming process of SA⁻···H₃O⁺ ion pair contained two steps: (i) SO₃ hydration along with SA formation and (ii) SA deprotonation. Specifically, as for step (i), at 0.70 ps, a transition state like structure of SO₃ hydration was observed with SO₃, SA⁻ and an interfacial water molecule involved. Note that at this time the H1 atom in interfacial H₂O molecule migrated to the O2 atom of SA⁻ ion instead of the surrounding water molecule. At 0.96 ps, the O1-H1 bond of H₂O was broken with the length of 1.56 Å, while the S1-O1 bond was formed with the length of 1.75 Å, demonstrating the completion of hydrolysis reaction of SO₃ and the formation of SA molecule. Then, at 8.08 ps, the H2 proton transferred from SA to the O4 atom of SA⁻ ion and to the O5 atom of the nearby water molecule was occurred, where the O3-H2 and O1-H3 bonds extended to 1.13 Å and 1.22 Å, and the length of O4-H2 and O5-H3 bonds shortened to 1.45 Å and 1.20 Å. Finally, SA deprotonation was completed at 8.23 ps with the formation of SA⁻···H₃O⁺ ion pair. During the whole indirect forming process of SA⁻···H₃O⁺ ion pair, SA⁻ played as protons donor and acceptor, and water molecules acted as hydration reactants and proton acceptors. Compared with the direct mechanism of SA⁻···H₃O⁺ ion pair, the indirect forming process of HSO₄⁻···H₃O⁺ ion pair required more time. This was consistent with the interfacial reactions of CH₂OO + HNO₃ (Kumar et al., 2018) and the hydration of SO₃ (Lv and Sun, 2020) where the direct forming mechanism needed less time than indirect forming mechanism.

The H₂S₂O₇ dissociating on water droplet. In addition to the gaseous SO₃ colliding with SA⁻ at the air-water interface, DSA, the product of the barrierless reaction between SO₃ and SA, can

further quickly react with interfacial water molecule at the air-water interface. As seen in Figure 4, Figure S7 and Movie S4, DSA was highly reactive at the air-water interface and can undergo two deprotonations to form $S_2O_7^{2-}$ ion. Specifically, the DSA can firstly form a H-bond with interfacial water molecule at 0.45 ps. After that, the H1 atom of DSA transferred to interfacial water and produced $HS_2O_7^-$ and H_3O^+ ions. The formed $HS_2O_7^-$ ion can survive for ~ 3 ps on water droplet. At 4.14 ps, the H2 atom of $HS_2O_7^-$ ion moved to O4 atom of nearby interfacial water molecule and produced the formation of $S_2O_7^{2-} \cdots H_3O^+$ ion pair, which was stable at the air-water interface over a simulated time scale of 10 ps. Note that the second deprotonation of DSA indeed needs more time than its first deprotonation as the pK_{a1} ($pK_{a1} = -16.05$) of DSA is much smaller than its pK_{a2} ($pK_{a2} = -4.81$) (Abedi and Farrokhpour, 2013). In brief, at the air-water interface, both these two routes of the formation of $S_2O_7^{2-} \cdots H_3O^+$ ion pair occurred on the picosecond time scale.

3.3 Atmospheric implications

The application of the $SO_3 + SA$ reaction in atmospheric chemistry. In the gas-phase, the main sink route of SO_3 was H_2O -assisted hydrolysis of SO_3 (Morokuma and Muguruma, 1994; Akhmatskaya et al., 1997; Larson et al., 2000; Hazra and Sinha, 2011; Long et al., 2013a; Torrent-Sucarrat et al., 2012; Ma et al., 2020). To study the atmospheric importance of the $SO_3 + SA$ reaction without and with H_2O , the rate ratio (v_{DSA}/v_{SA}) between the $SO_3 + SA$ reaction and H_2O -assisted hydrolysis of SO_3 was compared, which was expressed in Eq. (5).

$$\frac{v_{DSA}}{v_{SA}} = \frac{k_{DSA} \times [SO_3] \times [H_2SO_4] + k_{DSA_WM_s} \times K_{eq1} \times [SO_3] \times [H_2SO_4] \times [H_2O]}{k_{SA_WM} \times K_{eq2} \times [SO_3] \times [H_2O] \times [H_2O]} \quad (5)$$

In Eq. (5), K_{eq1} and K_{eq2} were the equilibrium constant for the formation of $H_2SO_4 \cdots H_2O$ and $SO_3 \cdots H_2O$ complexes shown in Table S2, respectively; k_{DSA} , $k_{DSA_WM_s}$ and k_{SA_WM} were respectively denoted the bimolecular rate coefficient for the $H_2SO_4 + SO_3$, $H_2SO_4 \cdots H_2O + SO_3$ and $SO_3 \cdots H_2O + H_2O$ reactions; $[H_2O]$ and $[H_2SO_4]$ were respectively represented the concentration of H_2O and SA taken from references (Anglada et al., 2013; Liu et al., 2015); The value of v_{DSA}/v_{SA} was listed in Table S7 (0 km altitude) and Table S8 (5-30 km altitude). As seen in Table S7, the hydrolysis reaction of SO_3 with $(H_2O)_2$ dominates over the $SO_3 + H_2SO_4$ reaction at 0 km altitude as the $[H_2O]$ (10^{16} - 10^{18} molecules \cdot cm 3) was much larger than that of $[H_2SO_4]$ (10^4 - 10^8 molecules \cdot cm 3). Although the concentration of water molecules decreased with the increasing of altitude in Table S8, the concentration of $[H_2O]$ was still much greater than that of $[H_2SO_4]$, resulting

in the $\text{SO}_3 + \text{H}_2\text{SO}_4$ reaction cannot compete with H_2O -assisted hydrolysis of SO_3 within the altitude range of 5-30 km. Even considering of high H_2SO_4 concentration at the end and outside the aircraft engine and flight at 10 km (Curtius et al., 2002), the $\text{SO}_3 + \text{H}_2\text{SO}_4$ reaction was not the major sink route of SO_3 . Notably, as the concentration of sulfuric acid was even greater than that of water vapor
385 in the atmosphere of Venus, the $\text{SO}_3 + \text{SA}$ reaction was probably favorable than the H_2O -assisted hydrolysis of SO_3 in the Venus' atmosphere. To check whether the $\text{SO}_3 + \text{H}_2\text{SO}_4$ reaction was more favorable than H_2O -assisted hydrolysis of SO_3 or not in the Venus' atmosphere, the rate ratio of $v_{\text{DSA}}/v_{\text{SA}}$ listed in Eq. 4 has been calculated in Table 2. It can be seen from Table 2 that the rate ratio of $v_{\text{DSA}}/v_{\text{SA}}$ was 3.24×10^8 - 5.23×10^{10} within the altitude range of 40-70 km in the Venus' atmosphere, which indicates that the $\text{SO}_3 + \text{H}_2\text{SO}_4$ reaction is significantly more favorable than the hydrolysis reaction of $\text{SO}_3 + (\text{H}_2\text{O})_2$ within the altitudes range of 40-70 km in the Venus' atmosphere.

Enhancement effect of DSA on NPF. From the multistep global minimum sampling technique, for $(\text{DSA})_x(\text{SA})_y(\text{A})_z$ ($z \leq x + y \leq 3$) molecular clusters, 27 most stable structures in the present system have been found (Figure S11). To evaluate the thermodynamic stability of these clusters,
395 Gibbs formation free energies (ΔG) at 278.15 K and evaporation rate coefficient (γ , s^{-1}) for $(\text{DSA})_x(\text{SA})_y(\text{A})_z$ ($z \leq x + y \leq 3$) molecular clusters were calculated in Figure 5 and Table S11-12, respectively. As for dimers formed by SA, A and DSA, the ΔG of $(\text{A})_1 \cdot (\text{DSA})_1$ was $-16.1 \text{ kcal} \cdot \text{mol}^{-1}$, which was lowest in all dimers followed by $(\text{SA})_2$ ($-8.5 \text{ kcal} \cdot \text{mol}^{-1}$) and then $(\text{SA})_1 \cdot (\text{A})_1$ ($-6.3 \text{ kcal} \cdot \text{mol}^{-1}$), meanwhile, the γ of $(\text{A})_1 \cdot (\text{DSA})_1$ ($1.17 \times 10^{-3} \text{ s}^{-1}$) was lower than those of $(\text{SA})_2$ (3.81
400 $\times 10^2 \text{ s}^{-1}$) and $(\text{SA})_1 \cdot (\text{A})_1$ ($4.19 \times 10^4 \text{ s}^{-1}$). Regarding for the SA-A-DSA-based clusters, the values of ΔG and γ of SA-A-DSA-based clusters containing more DSA molecules were relatively lower than the corresponding values of other SA-A-DSA-based clusters with the same number of acid and base molecules. In the free-energy diagram for cluster formation steps of the SA-A-DSA system (Figure 5), thermodynamic barriers were weakened mainly by the subsequential addition of A or
405 DSA monomer. Also, the SA-A-DSA-based growth pathway was thermodynamically favorable with decreasing ΔG . These results indicate that DSA not only can promote the stability of SA-A-DSA-based clusters but also may synergistically participate in the nucleation process.

The potential enhancement influence of DSA to the SA-A-based particle formation was shown in Figure 6. The formation rate (J , $\text{cm}^{-3} \cdot \text{s}^{-1}$) of SA-A-DSA-based system illustrated in Figure 6 was
410 negatively dependent on temperature, demonstrating that the low temperature is a key factor to

accelerate cluster formation. It is noted that, at low temperatures of 218.15 K (Figure S12) and 238.15 K (Figure S13), the actual ΔG of clusters has been calculated to ensure meaningful cluster dynamics of the 3×3 systems, where the actual ΔG surface represented that the simulated set of clusters always included the critical cluster. In addition to temperature, the J of SA-A-DSA-based system shown in Figure 6 rise with the increase of [DSA]. More notably, the participation of DSA can promote J to a higher level, indicating its enhancement on SA-A nucleation. Besides, there was significantly positive dependence of the J of SA-A-DSA-based system on both [SA] and [A] in Figure 7 (238.15 K) and Figure S15-Figure S18 (218.15, 258.15, 278.15 and 298.15 K). This was because the higher concentration of nucleation precursors could lead to higher J . Besides, Figure S19 showed the nucleation rate when the sum ([SA] + [DSA]) was kept constant. $J_{\text{DSA/SA}}$ at substituted condition was higher than that at unsubstituted condition. These results indicated that DSA may can greatly enhance the SA-A particle nucleation in heavy sulfur oxide polluted atmospheric boundary layer, especially at an average flight altitude of 10 km with high [DSA].

Two main cluster formation pathways, the pure SA-A-based cluster (*i*) and DSA-containing cluster (*ii*), at different [DSA] and different temperatures (218.15 K, 238.15 K and 258.15 K) were shown in Figure 8(a). As seen, the DSA molecule exhibited an ability to directly participate in cluster formation under high [SA] and [DSA], and median [A]. Interestingly, at different temperature and different [DSA], the DSA molecule showed different effect mechanism and contribution in SA-A system. As seen in Figure 8(b) and Figure S20(b), the cluster growth pathways were dominated by DSA-containing cluster formation under the conditions of 238.15 K ([DSA] is 10^6 - 10^7 molecules $\cdot\text{cm}^{-3}$), 258.15 K ([DSA] is 10^5 - 10^7 molecules $\cdot\text{cm}^{-3}$), 278.15 K ([DSA] is 10^4 - 10^7 molecules $\cdot\text{cm}^{-3}$) and 298.15 K ([DSA] is 10^4 - 10^7 molecules $\cdot\text{cm}^{-3}$). By the way, the cluster growth pathways were completely dominated by the DSA-containing cluster at 298.15 K where [DSA]= 10^5 - 10^7 molecules $\cdot\text{cm}^{-3}$, and its contribution for growth flux out of the system reached to 100% (Figure S22). In short, on one hand, the contribution of the DSA participation pathway has been increased with increasing temperature. On the other hand, the contribution of the pathway with participation of DSA increased with increasing [DSA], while the number of DSA molecules contained in clusters [(SA) $_2$ ·(A) $_3$ ·DSA, SA·(A) $_2$ ·DSA, SA·(A) $_3$ ·(DSA) $_2$, and (A) $_3$ ·(DSA) $_3$] that can contribute to cluster growth had a positive correlation with [DSA]. These results suggested that DSA has the ability to act as a potential contributor to SA-A-based NPF in the atmosphere at low T , low

[SA], high [A] and high [DSA], and the DSA participation pathway can be dominant in heavy sulfur oxide polluted atmospheric boundary layer and in season of late autumn and early winter.

At the air-water interface, important implication of the BOMD simulations was that the reaction between SO_3 and SA at the air-water interface can be accomplished within a few
445 picoseconds, among which the interfacial water molecules played a significant role in promoting the formation of $\text{S}_2\text{O}_7^{2-}\cdots\text{H}_3\text{O}^+$ and $\text{SA}^-\cdots\text{H}_3\text{O}^+$ ion pairs. Furthermore, the adsorption capacity of the $\text{S}_2\text{O}_7^{2-}$, H_3O^+ and SA^- to gaseous precursors in the atmosphere was further investigated by the calculated interaction free energies. Herein, the species of SA, NH_3 , HNO_3 and $(\text{COOH})_2$ have been regarded as the candidate species. (Kulmala et al., 2004; Kirkby et al., 2011). Our calculated Gibbs
450 free energies in Table 3 showed that the interactions of $\text{S}_2\text{O}_7^{2-}\cdots\text{H}_2\text{SO}_4$, $\text{S}_2\text{O}_7^{2-}\cdots\text{HNO}_3$, $\text{S}_2\text{O}_7^{2-}\cdots(\text{COOH})_2$, $\text{H}_3\text{O}^+\cdots\text{NH}_3$, $\text{H}_3\text{O}^+\cdots\text{H}_2\text{SO}_4$, $\text{SA}^-\cdots\text{H}_2\text{SO}_4$, $\text{SA}^-\cdots(\text{COOH})_2$, and $\text{SA}^-\cdots\text{HNO}_3$ were stronger than those of $\text{H}_2\text{SO}_4\cdots\text{NH}_3$ (major precursor of atmospheric aerosols) with their binding free energies enhanced by 18.6-42.8 $\text{kcal}\cdot\text{mol}^{-1}$. These results reveal that interfacial $\text{S}_2\text{O}_7^{2-}$, SA^- and H_3O^+ can attract candidate species from the gas phase to the water surface. **Moreover, we evaluated**
455 **whether $\text{S}_2\text{O}_7^{2-}$ could lead to increased particle growth on SA-A cluster by considering geometrical structure and the formation free energies of the $(\text{SA})_1(\text{A})_1(\text{S}_2\text{O}_7^{2-})_1$ clusters.** As compared with $(\text{SA})_1(\text{A})_1(\text{X})_1$ ($\text{X} = \text{HOOCCH}_2\text{COOH}$, $\text{HOCCOOSO}_3\text{H}$, $\text{CH}_3\text{OSO}_3\text{H}$, $\text{HOOCCH}_2\text{CH}(\text{NH}_2)\text{COOH}$ and HOCH_2COOH) clusters (Zhong et al., 2019; Zhang et al., 2018; Rong et al., 2020; Gao et al., 2023; Liu et al., 2021a; Zhang et al., 2017), the number of hydrogen bonds in $(\text{SA})_1(\text{A})_1(\text{S}_2\text{O}_7^{2-})_1$
460 cluster presented in Figure S8 increased and the ring of the complex was enlarged. It was demonstrated that $\text{S}_2\text{O}_7^{2-}$ has the highest potential to stabilize SA-A clusters and promote SA-A nucleation in these clusters due to its acidity and structural factors such as more intermolecular hydrogen bond binding sites. Subsequently, comparing to $(\text{SA})_1(\text{A})_1(\text{X})_1$ clusters (Table 2), the Gibbs formation free energy ΔG of $(\text{SA})_1(\text{A})_1(\text{S}_2\text{O}_7^{2-})_1$ cluster was lower, showing $\text{S}_2\text{O}_7^{2-}$ ion at the
465 air-water interface has stronger nucleation ability than X in the gas phase. Therefore, **we predict that $\text{S}_2\text{O}_7^{2-}$ at the air-water interface would lead to increased particle growth.**

4 Summary and conclusions

In this work, we employed QC calculations, BOMD simulations and ACDC kinetic model to characterize the SO_3 - H_2SO_4 interaction in the gas phase and at the air-water interface and to study

470 the effect of $\text{H}_2\text{S}_2\text{O}_7$ on $\text{H}_2\text{SO}_4\text{-NH}_3$ -based clusters. Results revealed that the energy barrier of the
gas phase $\text{SO}_3 + \text{H}_2\text{SO}_4$ reaction without and with H_2O was less than $2.3 \text{ kcal}\cdot\text{mol}^{-1}$. Rate constants
indicated that though the $\text{SO}_3 + \text{H}_2\text{SO}_4$ reaction cannot compete with H_2O -assisted hydrolysis of
 SO_3 within the temperature range of 280-320 K, its rate constant was close to the upper limits for
bimolecular reactions and H_2O exerted obvious catalytic role in promoting the reaction rate.
475 Moreover, ACDC kinetic simulations showed that DSA has unexpected facilitate effects on the NPF
process and can present a more obvious enhancement effect on SA-A-based cluster formation in
polluted atmospheric boundary layer. Of particular note, DSA can directly participate in the SA-A-
based cluster formation pathway and the contribution of the pathway with participation of DSA
increases with increasing [DSA] in regions with atmospheric pollution boundary layer of high
480 concentrations of SO_3 , especially in late autumn and early winter.

At the air-water interface, H_2O -induced the formation of $\text{S}_2\text{O}_7^{2-}\cdots\text{H}_3\text{O}^+$ ion pair, SA^- mediated
the formation of $\text{SA}^-\cdots\text{H}_3\text{O}^+$ ion pair and the deprotonation of $\text{H}_2\text{S}_2\text{O}_7$ were observed, both of which
can occur within a few picoseconds. The formed interfacial $\text{S}_2\text{O}_7^{2-}$, SA^- and H_3O^+ can attract
candidate species (such as H_2SO_4 , NH_3 , and HNO_3) for particle formation from the gas phase to the
485 water surface, and thus accelerated the growth of particle. Moreover, potential of X ($X = \text{S}_2\text{O}_7^{2-}$,
 $\text{HOOCCH}_2\text{COOH}$, $\text{HOCCOOSO}_3\text{H}$, $\text{CH}_3\text{OSO}_3\text{H}$, $\text{HOOCCH}_2\text{CH}(\text{NH}_2)\text{COOH}$ and HOCH_2COOH)
in ternary SA-A- X cluster formation indicated that $\text{S}_2\text{O}_7^{2-}$ has the highest potential to stabilize SA-
A clusters and promote SA-A nucleation among X .

The present work will expand our understanding of new pathway for the loss of SO_3 in acidic
490 polluted areas. Moreover, this work will also help to reveal some missing sources of metropolis
industrial regions NPF and to understand the atmospheric organic-sulfur cycle more
comprehensively.

Data availability

All data presented in this study are available upon request from the corresponding author.

495 Acknowledgments

This work was supported by the National Natural Science Foundation of China (No: 22203052;
22073059; 22006158); the Education Department of Shaanxi Provincial Government (no. 23JC023),
the Key Cultivation Project of Shaanxi University of Technology (No: SLG2101); The Special
Scientific Research Project of Hanzhong City-Shaanxi University of Technology Co-construction

500 State Key Laboratory (SXJ-2106); The authors thank Prof. Qingzhu Zhang and Fei Xu from Shandong University for their sincere assistance in calculating the air-water interface reaction.

Declaration of competing interest

The authors declare that they have no known competing financial interests or personal relationships that could have appeared to influence the work reported in this paper.

505 Reference

- Abedi, M., and Farrokhpour, H.: Acidity constants of some sulfur oxoacids in aqueous solution using CCSD and MP2 methods, *Dalton Trans.*, 42, 5566-5572, 10.1039/C3DT33056G, 2013.
- Adler, T. B., Knizia, G., and Werner, H. J.: A simple and efficient CCSD(T)-F12 approximation, *J. Chem. Phys.*, 127, 221106, 10.1063/1.2817618, 2007.
- 510 Akhmatkaya, E., Apps, C., Hillier, I., Masters, A., Palmer, I., Watt, N., Vincent, M., and Whitehead, J.: Hydrolysis of SO₃ and ClONO₂ in water clusters A combined experimental and theoretical study, *J. Am. Chem. Soc.*, 93, 2775-2779, 1997.
- Almeida, J., Schobesberger, S., Kürten, A., Ortega, I. K., Kupiainen-Määttä, O., Praplan, A. P., Adamov, A., Amorim, A., Bianchi, F., Breitenlechner, M., David, A., Dommen, J., Donahue, N. M., Downard, A., Dunne, E., Duplissy, J., Ehrhart, S., Flagan, R. C., Franchin, A., Guida, R., Hakala, J., Hansel, A., Heinritzi, M., Henschel, H., Jokinen, T., Junninen, H., Kajos, M., Kangasluoma, J., Keskinen, H., Kupc, A., Kurtén, T., Kvashin, A. N., Laaksonen, A., Lehtipalo, K., Leiminger, M., Leppä, J., Loukonen, V., Makhmutov, V., Mathot, S., McGrath, M. J., Nieminen, T., Olenius, T., Onnela, A., Petäjä, T., Riccobono, F., Riipinen, I., Rissanen, M., Rondo, L., Ruuskanen, T., Santos, F. D., Sarnela, N., Schallhart, S., Schnitzhofer, R., Seinfeld, J. H., Simon, M., Sipilä, M., Stozhkov, Y., Stratmann, F., Tomé, A., Tröstl, J., Tsagkogeorgas, G., Vaattovaara, P., Viisanen, Y., Virtanen, A., Vrtala, A., Wagner, P. E., Weingartner, E., Wex, H., Williamson, C., Wimmer, D., Ye, P., Yli-Juuti, T., Carslaw, K. S., Kulmala, M., Curtius, J., Baltensperger, U., Worsnop, D. R., Vehkamäki, H., and Kirkby, J.: Molecular understanding of sulphuric acid–amine particle nucleation in the atmosphere, *Nature*, 520, 359-363, 10.1038/nature12663, 2013.
- 525 Anglada, J. M., Hoffman, G. J., Slipchenko, L. V., M. Costa, M., Ruiz-Lopez, M. F., and Francisco, J. S.: Atmospheric significance of water clusters and ozone-water complexes, *J. Phys. Chem. A*, 117, 10381-10396, 2013.
- Bandyopadhyay, B., Kumar, P., and Biswas, P.: Ammonia Catalyzed Formation of Sulfuric Acid in Troposphere: The Curious Case of a Base Promoting Acid Rain, *J. Phys. Chem. A*, 121, 3101-3108, 10.1021/acs.jpca.7b01172, 2017.
- 530 Becke, A. D.: Density-functional exchange-energy approximation with correct asymptotic behavior, *Phys. Rev. A*, 38, 3098-3100, 1988.
- Bouo, F.-X., Kouamé, J., Tchétché, Y., Kré, R., Moussé, M., Assamoi, P., Cautenet, S., and Cautenet, G.: Redistribution of free tropospheric chemical species over West Africa: Radicals (OH and HO₂), peroxide (H₂O₂) and acids (HNO₃ and H₂SO₄), *Chemosphere*, 84, 1617-1629, 2011.
- Calvert, J. G., Lazrus, A., Kok, G. L., Heikes, B. G., Walega, J. G., Lind, J., and Cantrell, C. A.: Chemical mechanisms of acid generation in the troposphere, *Nature*, 317, 27-35, 1985.

- 540 Cao, Y., Zhou, H., Jiang, W., Chen, C. W., and Pan, W. P.: Studies of the fate of sulfur trioxide in coal-fired utility boilers based on modified selected condensation methods, *Environ. Sci. Technol.*, 44, 3429-3434, 2010.
- Chen, L., and Bhattacharya, S.: Sulfur emission from Victorian brown coal under pyrolysis, oxy-fuel combustion and gasification conditions, *Environ. Sci. Technol.*, 47, 1729-1734, 2013.
- 545 Chen, T., and Plummer, P. L.: Ab initio MO investigation of the gas-phase reaction sulfur trioxide + water. *J. Phys. Chem. A*, 89, 3689-3693, 1985.
- Chen, X., Tao, C., Zhong, L., Gao, Y., Yao, W., and Li, S.: Theoretical study on the atmospheric reaction of SO₂ with the HO₂ and HO₂·H₂O complex formation HSO₄ and H₂SO₃, *Chem. Phys. Lett.*, 608, 272-276, 2014.
- 550 Cheng, Y., Ding, C., Wang, H., Zhang, T., Wang, R., Muthiah, B., Xu, H., Zhang, Q., and Jiang, M.: Significant influence of water molecules on the SO₃ + HCl reaction in the gas phase and at the air-water interface, *Phys. Chem. Chem. Phys.*, 25, 28885-28894, 10.1039/D3CP03172A, 2023.
- Curtius, J., Arnold, F., and Schulte, P.: Sulfuric acid measurements in the exhaust plume of a jet aircraft in flight: Implications for the sulfuric acid formation efficiency, *Geophys. Res. Lett.*, 29, 17-11-17-14, 2002.
- 555 Elm, J., Bilde, M., and Mikkelsen, K. V.: Assessment of density functional theory in predicting structures and free energies of reaction of atmospheric prenucleation clusters, *J. Chem. Theory Comput.*, 8, 2071-2077, 2012.
- Elm, J., Bilde, M., and Mikkelsen, K. V.: Influence of nucleation precursors on the reaction kinetics of methanol with the OH radical, *J. Phys. Chem. A*, 117, 6695-6701, 2013.
- 560 England, G. C., Zielinska, B., Loos, K., Crane, I., and Ritter, K.: Characterizing PM_{2.5} emission profiles for stationary sources: comparison of traditional and dilution sampling techniques, *Fuel Process. Technol.*, 65, 177-188, 2000.
- Finlayson-Pitts, B. J., and Pitts Jr, J. N.: *Atmospheric chemistry. Fundamentals and experimental techniques*, John Wiley and Sons: New York, 1986.
- 565 Frisch, M. J., Trucks, G. W., Schlegel, H. B., Scuseria, G. E., Robb, M. A., Cheeseman, J. R., Scalmani, G., Barone, V., Mennucci, B., Petersson, G. A., Nakatsuji, H., Caricato, M., Li, X., Hratchian, H. P., Izmaylov, A. F., Bloino, J., Zheng, G., Sonnenberg, J. L., Hada, M., Ehara, M., Toyota, K., Fukuda, R., Hasegawa, J., Ishida, M., Nakajima, T., Honda, Y., Kitao, O., Nakai, H., Vreven, T., Montgomery, J. A., Jr., Peralta, J. E., Ogliaro, F., Bearpark, M., Heyd, J. J., Brothers, E., Kudin, K. N., Staroverov, V. N., Kobayashi, R., Normand, J., Raghavachari, K., Rendell, A., Burant, J. C., Iyengar, S. S., Tomasi, J., Cossi, M., Rega, N., Millam, J. M., Klene, M., Knox, J. E., Cross, J. B., Bakken, V., Adamo, C., Jaramillo, J., Gomperts, R., Stratmann, R. E., Yazyev, O., Austin, A. J., Cammi, R., Pomelli, C., Ochterski, J. W., Martin, R. L., Morokuma, K., Zakrzewski, V. G., Voth, G. A., Salvador, P., Dannenberg, J. J., Dapprich, S., Daniels, A. D., Farkas, Ö., Foresman, J. B., Ortiz, J. V.,
- 575 Cioslowski, J., and Fox, D. J.: Gaussian09 Revision D. 01, Gaussian Inc. Wallingford CT, See also: URL: <http://www.gaussian.com>, 2009.
- Gao, J., Wang, R., Zhang, T., Liu, F., and Wang, W.: Effect of methyl hydrogen sulfate on the formation of sulfuric acid-ammonia clusters: A theoretical study, *J. Chin. Chem. Soc.*, 70, 689-698, <https://doi.org/10.1002/jccs.202200148>, 2023.
- 580 Glowacki, D. R., Liang, C.-H., Morley, C., Pilling, M. J., and Robertson, S. H.: MESMER: an open-source master equation solver for multi-energy well reactions, *J. Phys. Chem. A*, 116, 9545-9560, 2012.

- Goedecker, S., Teter, M., and Hutter, J.: Separable dual-space Gaussian pseudopotentials, *Phys. Rev. B*, 54, 1703, 1996.
- 585 Gonzalez, J., Torrent-Sucarrat, M., and Anglada, J. M.: The reactions of SO₃ with HO₂ radical and H₂O··HO₂ radical complex. Theoretical study on the atmospheric formation of HSO₅ and H₂SO₄, *Phys. Chem. Chem. Phys.*, 12, 2116-2125, 2010.
- Grimme, S., Antony, J., Ehrlich, S., and Krieg, H.: A consistent and accurate ab initio parametrization of density functional dispersion correction (DFT-D) for the 94 elements H-Pu, *J. Chem. Phys.*, 132, 154104, 2010.
- 590 Hartwigsen, C., Goedecker, S., and Hutter, J.: Relativistic separable dual-space Gaussian pseudopotentials from H to Rn, *Phys. Rev. B*, 58, 3641-3662, 1998.
- Haywood, J., and Boucher, O.: Estimates of the direct and indirect radiative forcing due to tropospheric aerosols: A review, *Rev. Geophys.*, 38, 513-543, 2000.
- 595 Hazra, M. K., and Sinha, A.: Formic acid catalyzed hydrolysis of SO₃ in the gas phase: A barrierless mechanism for sulfuric acid production of potential atmospheric importance, *J. Am. Chem. Soc.*, 133, 17444-17453, 2011.
- Hofmann, M., and Schleyer, P. v. R.: Acid rain: Ab initio investigation of the H₂O•SO₃ complex and its conversion to H₂SO₄, *J. Am. Chem. Soc.*, 116, 4947-4952, 1994.
- 600 Horváth, G., Horváth, I., Almousa, S. A.-D., and Telek, M.: Numerical inverse Laplace transformation using concentrated matrix exponential distributions, *Perform. Evaluation*, 137, 102067, 2020.
- Huff, A. K., Mackenzie, R. B., Smith, C. J., and Leopold, K. R.: Facile Formation of Acetic Sulfuric Anhydride: Microwave Spectrum, Internal Rotation, and Theoretical Calculations, *J. Phys. Chem. A*, 121, 5659-5664, 10.1021/acs.jpca.7b05105, 2017.
- 605 Hutter, J., Iannuzzi, M., Schiffrmann, F., and VandeVondele, J.: *Wiley Interdiscip. Wiley Interdiscip. Rev. Comput. Mol. Sci.*, 4, 15-25, 2014.
- Kanno, N., Tonokura, K., and Koshi, M.: Equilibrium constant of the HO₂-H₂O complex formation and kinetics of HO₂ + HO₂-H₂O: Implications for tropospheric chemistry, *J. Geophys. Res.: Atmos.*, 111, 10.1029/2005jd006805, 2006.
- 610 Kikuchi, R.: Environmental management of sulfur trioxide emission: impact of SO₃ on human health, *Environ. Manage.*, 27, 837-844, 2001.
- Kirkby, J., Curtius, J., Almeida, J., Dunne, E., Duplissy, J., Ehrhart, S., Franchin, A., Gagné, S., Ickes, L., Kürten, A., Kupc, A., Metzger, A., Riccobono, F., Rondo, L., Schobesberger, S., Tsagkogeorgas, G., Wimmer, D., Amorim, A., Bianchi, F., Breitenlechner, M., David, A., Dommen, J., Downard, A., Ehn, M., Flagan, R. C., Haider, S., Hansel, A., Hauser, D., Jud, W., Junninen, H., Kreissl, F., Kvashin, A., Laaksonen, A., Lehtipalo, K., Lima, J., Lovejoy, E. R., Makhmutov, V., Mathot, S., Mikkilä, J., Minginette, P., Mogo, S., Nieminen, T., Onnela, A., Pereira, P., Petäjä, T., Schnitzhofer, R., Seinfeld, J. H., Sipilä, M., Stozhkov, Y., Stratmann, F., Tomé, A., Vanhanen, J., Viisanen, Y., Vrtala, A., Wagner, P. E., Walther, H., Weingartner, E., Wex, H., Winkler, P. M., Carslaw, K. S., Worsnop, D. R., Baltensperger, U., and Kulmala, M.: Role of sulphuric acid, ammonia and galactic cosmic rays in atmospheric aerosol nucleation, *Nature*, 476, 429-433, 10.1038/nature10343, 2011.
- 620 Knizia, G., Adler, T. B., and Werner, H.-J.: Simplified CCSD(T)-F12 methods: Theory and benchmarks, *J. Chem. Phys.*, 130, 054104, 10.1063/1.3054300, 2009.
- Kuang, C., McMurry, P. H., McCormick, A. V., and Eisele, F.: Dependence of nucleation rates on sulfuric acid vapor concentration in diverse atmospheric locations, *J. Geophys. Res. Atmos.*, 113, 2008.
- 625

- Kuczowski, R. L., Suenram, R. D., and Lovas, F. J.: Microwave spectrum, structure, and dipole moment of sulfuric acid, *J. Am. Chem. Soc.*, 103, 2561-2566, 1981.
- Kulmala, M., Vehkamäki, H., Petäjä, T., Dal Maso, M., Lauri, A., Kerminen, V. M., Birmili, W., and McMurry, P. H.: Formation and growth rates of ultrafine atmospheric particles: a review of observations, *J. Aerosol Sci.*, 35, 143-176, <https://doi.org/10.1016/j.jaerosci.2003.10.003>, 2004.
- 630 Kumar, M., Zhong, J., Francisco, J. S., and Zeng, X. C.: Criegee intermediate-hydrogen sulfide chemistry at the air/water interface, *Chem. Sci.*, 8, 5385-5391, 2017.
- Kumar, M., Zhong, J., Zeng, X. C., and Francisco, J. S.: Reaction of Criegee Intermediate with Nitric Acid at the Air-Water Interface, *J. Am. Chem. Soc.*, 140, 4913-4921, [10.1021/jacs.8b01191](https://doi.org/10.1021/jacs.8b01191), 2018.
- 635 Larson, L. J., Kuno, M., and Tao, F.-M.: Hydrolysis of sulfur trioxide to form sulfuric acid in small water clusters, *J. Chem. Phys.*, 112, 8830-8838, 2000.
- Lee, C., Yang, W., and Parr, R. G.: Development of the Colle-Salvetti correlation-energy formula into a functional of the electron density, *Phys. Rev. B*, 37, 785-789, 1988.
- Li, H., Zhong, J., Vehkamäki, H., Kurtén, T., Wang, W., Ge, M., Zhang, S., Li, Z., Zhang, X., Francisco, J. S., and Zeng, X. C.: Self-Catalytic Reaction of SO₃ and NH₃ To Produce Sulfamic Acid and Its Implication to Atmospheric Particle Formation, *J. Am. Chem. Soc.*, 140, 11020-11028, [10.1021/jacs.8b04928](https://doi.org/10.1021/jacs.8b04928), 2018a.
- 640 Li, K., Song, X., Zhu, T., Wang, C., Sun, X., Ning, P., and Tang, L.: Mechanistic and kinetic study on the catalytic hydrolysis of COS in small clusters of sulfuric acid, *Environ. Pollut.*, 232, 615-623, [10.1016/j.envpol.2017.10.004](https://doi.org/10.1016/j.envpol.2017.10.004), 2018b.
- 645 Li, L., Kumar, M., Zhu, C., Zhong, J., Francisco, J. S., and Zeng, X. C.: Near-barrierless ammonium bisulfate formation via a loop-structure promoted proton-transfer mechanism on the surface of water, *J. Am. Chem. Soc.*, 138, 1816-1819, 2016.
- Liu, J., Fang, S., Wang, Z., Yi, W., Tao, F. M., and Liu, J. Y.: Hydrolysis of sulfur dioxide in small clusters of sulfuric acid: Mechanistic and kinetic study, *Environ. Sci. Technol.*, 49, 13112-13120, 2015.
- 650 Liu, J., Liu, L., Rong, H., and Zhang, X.: The potential mechanism of atmospheric new particle formation involving amino acids with multiple functional groups, *Phys. Chem. Chem. Phys.*, 23, 10184-10195, [10.1039/D0CP06472F](https://doi.org/10.1039/D0CP06472F), 2021a.
- Liu, L., Zhong, J., Vehkamäki, H., Kurtén, T., Du, L., Zhang, X., Francisco, J. S., and Zeng, X. C.: Unexpected quenching effect on new particle formation from the atmospheric reaction of methanol with SO₃, *Proc. Natl. Acad. Sci. U.S.A.*, 116, 24966-24971, 2019.
- 655 Liu, L., Yu, F., Tu, K., Yang, Z., and Zhang, X.: Influence of atmospheric conditions on the role of trifluoroacetic acid in atmospheric sulfuric acid-dimethylamine nucleation, *Atmos. Chem. Phys.*, 21, 6221-6230, [10.5194/acp-21-6221-2021](https://doi.org/10.5194/acp-21-6221-2021), 2021b.
- 660 Loerting, T., and Liedl, K. R.: Toward elimination of discrepancies between theory and experiment: The rate constant of the atmospheric conversion of SO₃ to H₂SO₄, *Proc. Natl. Acad. Sci. U. S. A.*, 97, 8874-8878, 2000.
- Lohmann, U., and Feichter, J.: Global indirect aerosol effects: a review, *J. Atmos. Chem. Phys.*, 5, 715-737, 2005.
- 665 Long, B., Long, Z. W., Wang, Y.-b., Tan, X. F., Han, Y. H., Long, C. Y., Qin, S. J., and Zhang, W. J.: Formic Acid Catalyzed Gas-Phase Reaction of H₂O with SO₃ and the Reverse Reaction: A Theoretical Study, *ChemPhysChem*, 13, 323-329, [10.1002/cphc.201100558](https://doi.org/10.1002/cphc.201100558), 2012.

- Long, B., Chang, C. R., Long, Z. W., Wang, Y. B., Tan, X. F., and Zhang, W. J.: Nitric acid catalyzed hydrolysis of SO₃ in the formation of sulfuric acid: A theoretical study, *Chem. Phys. Lett.*, 581, 26-29, 2013a.
- 670 Long, B., Tan, X. F., Chang, C. R., Zhao, W. X., Long, Z. W., Ren, D. S., and Zhang, W. J.: Theoretical studies on gas-phase reactions of sulfuric acid catalyzed hydrolysis of formaldehyde and formaldehyde with sulfuric acid and H₂SO₄···H₂O complex, *J. Phys. Chem. A* 117, 5106-5116, 2013b.
- 675 Lv, G., and Sun, X. M.: The role of air-water interface in the SO₃ hydration reaction, 230, 117514, 2020.
- Lv, G., Sun, X., Zhang, C., and Li, M.: Understanding the catalytic role of oxalic acid in SO₃ hydration to form H₂SO₄ in the atmosphere, *Atmos. Chem. Phys.*, 19, 2833-2844, 2019.
- Ma, X., Zhao, X., Ding, Z., Wang, W., Wei, Y., Xu, F., Zhang, Q., and Wang, W.: Determination of the amine-catalyzed SO₃ hydrolysis mechanism in the gas phase and at the air-water interface, *Chemosphere*, 252, 126292, 2020.
- 680 Mackenzie, R. B., Dewberry, C. T., and Leopold, K. R.: Gas phase observation and microwave spectroscopic characterization of formic sulfuric anhydride, *Science*, 349, 58-61, 2015.
- MacKerell, A. D., Bashford, D., Bellott, M., Dunbrack, R. L., Evanseck, J. D., Field, M. J., Fischer, S., Gao, J., Guo, H., Ha, S., Joseph-McCarthy, D., Kuchnir, L., Kuczera, K., Lau, F. T. K., Mattos, C., Michnick, S., Ngo, T., Nguyen, D. T., Prodhom, B., Reiher, W. E., Roux, B., Schlenkrich, M., Smith, J. C., Stote, R., Straub, J., Watanabe, M., Wiórkiewicz-Kuczera, J., Yin, D., and Karplus, M.: All-Atom Empirical Potential for Molecular Modeling and Dynamics Studies of Proteins, *J. Phys. Chem. B*, 102, 3586-3616, 10.1021/jp973084f, 1998.
- 685 Mardirossian, N., and Head-Gordon, M.: How accurate are the Minnesota density functionals for noncovalent interactions, isomerization energies, thermochemistry, and barrier heights involving molecules composed of main-group elements?, *J. Chem. Theory Comput.*, 12, 4303-4325, 2016.
- McGrath, M. J., Olenius, T., Ortega, I. K., Loukonen, V., Paasonen, P., Kurtén, T., Kulmala, M., and Vehkamäki, H.: Atmospheric Cluster Dynamics Code: a flexible method for solution of the birth-death equations, *Atmos. Chem. Phys.*, 12, 2345-2355, 10.5194/acp-12-2345-2012, 2012.
- 695 Miller, J. A., and Klippenstein, S. J.: Master equation methods in gas phase chemical kinetics, *J. Phys. Chem. A*, 110, 10528-10544, 2006.
- Mitsui, Y., Imada, N., Kikkawa, H., and Katagawa, A.: Study of Hg and SO₃ behavior in flue gas of oxy-fuel combustion system, *Int. J. Greenhouse Gas Control*, 5, S143-S150, 2011.
- Morokuma, K., and Muguruma, C.: Ab initio molecular orbital study of the mechanism of the gas phase reaction SO₃ + H₂O: Importance of the second water molecule, *J. Am. Chem. Soc.*, 116, 10316-10317, 1994.
- 700 Neese, F.: The ORCA program system, *WIREs Comput. Mol. Sci.*, 2, 73-78, <https://doi.org/10.1002/wcms.81>, 2012.
- Otto, A. H., and Steudel, R.: Gas-Phase Structures and Acidities of the Sulfur Oxoacids H₂S_nO₆ (*n* = 2-4) and H₂S₂O₇, *Eur. J. Inorg. Chem.*, 2001, 3047-3054, 2001.
- 705 Pérez-Ríos, J., Ragole, S., Wang, J., and Greene, C. H.: Comparison of classical and quantal calculations of helium three-body recombination, *J. Chem. Phys.*, 140, 044307, 2014.
- Pöschl, U.: Atmospheric aerosols: composition, transformation, climate and health effects, *Angew. Chem., Int. Ed. Engl.*, 44, 7520-7540, 2005.
- 710 Pöschl, U., and Shiraiwa, M.: Multiphase chemistry at the atmosphere-biosphere interface influencing climate and public health in the anthropocene, *Chem. Rev.*, 115, 4440-4475, 2015.

- Renard, J. J., Calidonna, S. E., and Henley, M. V.: Fate of ammonia in the atmosphere-a review for applicability to hazardous releases, *J. Hazard. Mater.*, 108, 29-60, 2004.
- 715 Riipinen, I., Sihto, S.-L., Kulmala, M., Arnold, F., Dal Maso, M., Birmili, W., Saarnio, K., Teinilä, K., Kerminen, V.-M., and Laaksonen, A.: Connections between atmospheric sulphuric acid and new particle formation during QUEST III-IV campaigns in Heidelberg and Hyytiälä, *Atmos. Chem. Phys.*, 7, 1899-1914, 2007.
- 720 Rong, H., Liu, L., Liu, J., and Zhang, X.: Glyoxylic sulfuric anhydride from the gas-phase reaction between glyoxylic acid and SO₃: a potential nucleation precursor, *J. Phys. Chem. A*, 124, 3261-3268, 2020.
- Shampine, L. F., and Reichelt, M. W.: The MATLAB ODE Suite, *J. Sci. Comput.*, 18, 1-22, 10.1137/s1064827594276424, 1997.
- 725 Sihto, S.-L., Kulmala, M., Kerminen, V.-M., Dal Maso, M., Petäjä, T., Riipinen, I., Korhonen, H., Arnold, F., Janson, R., and Boy, M.: Atmospheric sulphuric acid and aerosol formation: implications from atmospheric measurements for nucleation and early growth mechanisms, *Atmos. Chem. Phys.*, 6, 4079-4091, 2006.
- Sipilä, M., Berndt, T., Petäjä, T., Brus, D., Vanhanen, J., Stratmann, F., Patokoski, J., Mauldin III, R. L., Hyvärinen, A.-P., and Lihavainen, H.: The role of sulfuric acid in atmospheric nucleation, *Science*, 327, 1243-1246, 2010.
- 730 Smith, C. J., Huff, A. K., Mackenzie, R. B., and Leopold, K. R.: Observation of Two Conformers of Acrylic Sulfuric Anhydride by Microwave Spectroscopy, *J. Phys. Chem. A*, 121, 9074-9080, 10.1021/acs.jpca.7b09833, 2017.
- 735 Starik, A., Savel'Ev, A., Titova, N., Loukhovitskaya, E., and Schumann, U.: Effect of aerosol precursors from gas turbine engines on the volatile sulfate aerosols and ion clusters formation in aircraft plumes, *Phys. Chem. Chem. Phys.*, 6, 3426-3436, 2004.
- Stedel, R.: Sulfuric acid from sulfur trioxide and water-a surprisingly complex reaction, *Angew. Chem. Int. Ed. Engl.*, 34, 1313-1315, 1995.
- Stewart, J.: MOPAC2016 Stewart computational chemistry. Colorado Springs, CO: OpenMOPAC, in, 2016.
- 740 Stewart, J. J.: Optimization of parameters for semiempirical methods VI: more modifications to the NDDO approximations and re-optimization of parameters, *J Mol Model*, 19, 1-32, 10.1007/s00894-012-1667-x, 2013.
- 745 Stewart, J. J. P.: Optimization of parameters for semiempirical methods V: Modification of NDDO approximations and application to 70 elements, *Journal of Molecular Modeling*, 13, 1173-1213, 10.1007/s00894-007-0233-4, 2007.
- Stone, D., and Rowley, D. M.: Kinetics of the gas phase HO₂ self-reaction: Effects of temperature, pressure, water and methanol vapours, *Phys. Chem. Chem. Phys.*, 7, 2156-2163, 10.1039/B502673C, 2005.
- 750 Tan, X. F., Long, B., Ren, D. S., Zhang, W. J., Long, Z. W., and Mitchell, E.: Atmospheric chemistry of CH₃CHO: the hydrolysis of CH₃CHO catalyzed by H₂SO₄, *Phys. Chem. Chem. Phys.*, 20, 7701-7709, 2018.
- Tilgner, A., Schaefer, T., Alexander, B., Barth, M., Collett Jr, J. L., Fahey, K. M., Nenes, A., Pye, H. O., Herrmann, H., and McNeill, V. F.: Acidity and the multiphase chemistry of atmospheric aqueous particles and clouds, *Atmos. Chem. Phys.*, 21, 13483-13536, 2021.

- 755 Torrent-Sucarrat, M., Francisco, J. S., and Anglada, J. M.: Sulfuric acid as autocatalyst in the formation of sulfuric acid, *J. Am. Chem. Soc.*, 134, 20632-20644, 2012.
- VandeVondele, J., and Hutter, J.: Gaussian basis sets for accurate calculations on molecular systems in gas and condensed phases, *J. Chem. Phys.*, 127, 114105, 2007.
- Viegas, L. P., and Varandas, A. J.: Can water be a catalyst on the $\text{HO}_2 + \text{H}_2\text{O} + \text{O}_3$ reactive cluster?, *Chem. Phys.*, 399, 17-22, 2012.
- 760 Viegas, L. P., and Varandas, A. J.: The $\text{HO}_2 + (\text{H}_2\text{O})_n + \text{O}_3$ reaction: an overview and recent developments, *Eur. Phys. J. D*, 70, 1-9, 2016.
- Wayne, R. P.: *Chemistry of Atmospheres. An Introduction to the Chemistry of the Atmospheres of Earth, the Planets, and Their Satellites*, 3rd Oxford University Press, 10.1021/ja004780n, 2000.
- 765 Weber, R., McMurry, P., Eisele, F., and Tanner, D.: Measurement of expected nucleation precursor species and 3-500-nm diameter particles at Mauna Loa observatory, Hawaii, *J. Atmos. Sci.*, 52, 2242-2257, 1995.
- Weber, R., Marti, J., McMurry, P., Eisele, F., Tanner, D., and Jefferson, A.: Measured atmospheric new particle formation rates: Implications for nucleation mechanisms, *Chem. Eng. Commun.*, 151, 53-64, 1996.
- 770 Weber, R., Chen, G., Davis, D., Mauldin III, R., Tanner, D., Eisele, F., Clarke, A., Thornton, D., and Bandy, A.: Measurements of enhanced H_2SO_4 and 3-4 nm particles near a frontal cloud during the First Aerosol Characterization Experiment (ACE 1), *J. Geophys. Res. Atmos.*, 106, 24107-24117, 2001.
- 775 Yang, Y., Liu, L., Wang, H., and Zhang, X.: Molecular-Scale Mechanism of Sequential Reaction of Oxalic Acid with SO_3 : Potential Participator in Atmospheric Aerosol Nucleation, *J. Phys. Chem. A*, 125, 4200-4208, 2021.
- Yao, L., Garmash, O., Bianchi, F., Zheng, J., Yan, C., Kontkanen, J., Junninen, H., Mazon, S. B., Ehn, M., Paasonen, P., Sipilä, M., Wang, M., Wang, X., Xiao, S., Chen, H., Lu, Y., Zhang, B., Wang, D., Fu, Q., Geng, F., Li, L., Wang, H., Qiao, L., Yang, X., Chen, J., Kerminen, V.-M., Petäjä, T., Worsnop, D. R., Kulmala, M., and Wang, L.: Atmospheric new particle formation from sulfuric acid and amines in a Chinese megacity, *Science*, 361, 278-281, doi:10.1126/science.aao4839, 2018.
- 780 Yao, L., Fan, X., Yan, C., Kurtén, T., Daellenbach, K. R., Li, C., Wang, Y., Guo, Y., Dada, L., Rissanen, M. P., Cai, J., Tham, Y. J., Zha, Q., Zhang, S., Du, W., Yu, M., Zheng, F., Zhou, Y., Kontkanen, J., Chan, T., Shen, J., Kujansuu, J. T., Kangasluoma, J., Jiang, J., Wang, L., Worsnop, D. R., Petäjä, T., Kerminen, V. M., Liu, Y., Chu, B., He, H., Kulmala, M., and Bianchi, F.: Unprecedented Ambient Sulfur Trioxide (SO_3) Detection: Possible Formation Mechanism and Atmospheric Implications, *Environ. Sci. Technol. Lett.*, 7, 809-818, 10.1021/acs.estlett.0c00615, 2020.
- 785 Zhao, Y., and Truhlar, D. G.: The M06 suite of density functionals for main group thermochemistry, thermochemical kinetics, noncovalent interactions, excited states, and transition elements: two new functionals and systematic testing of four M06-class functionals and 12 other functionals, *Theor. Chem. Acc.*, 120, 215-241, 2008.
- 790 Zhang, H., Kupiainen-Määttä, O., Zhang, X., Molinero, V., Zhang, Y., and Li, Z.: The enhancement mechanism of glycolic acid on the formation of atmospheric sulfuric acid-ammonia molecular clusters, *J. Chem. Phys.*, 146, 184308, 10.1063/1.4982929, 2017.
- 795 Zhang, H., Li, H., Liu, L., Zhang, Y., Zhang, X., and Li, Z.: The potential role of malonic acid in the atmospheric sulfuric acid-ammonia clusters formation, *Chemosphere*, 203, 26-33, 2018.

- Zhang, J., and Dolg, M.: ABCluster: the artificial bee colony algorithm for cluster global optimization, *Phys. Chem. Chem. Phys.*, 17, 24173-24181, 10.1039/C5CP04060D, 2015.
- 800 Zhang, J., and Dolg, M.: Global optimization of clusters of rigid molecules using the artificial bee colony algorithm, *Phys. Chem. Chem. Phys.*, 18, 3003-3010, 10.1039/C5CP06313B, 2016.
- Zhang, R., Khalizov, A., Wang, L., Hu, M., and Xu, W.: Nucleation and growth of nanoparticles in the atmosphere, *Chem. Rev.*, 112, 1957-2011, 2012.
- Zhang, R., Wang, G., Guo, S., Zamora, M. L., Ying, Q., Lin, Y., Wang, W., Hu, M., and Wang, Y.:
805 Formation of urban fine particulate matter, *Chem. Rev.*, 115, 3803-3855, 2015.
- Zhang, R., Shen, J., Xie, H. B., Chen, J., and Elm, J.: The role of organic acids in new particle formation from methanesulfonic acid and methylamine, *Atmos. Chem. Phys.*, 22, 2639-2650, 10.5194/acp-22-2639-2022, 2022.
- Zhong, J., Kumar, M., Zhu, C. Q., Francisco, J. S., and Zeng, X. C.: Frontispiece: Surprising Stability of
810 Larger Criegee Intermediates on Aqueous Interfaces, *Angew. Chem. Int. Ed.*, 56, 7740-7744, 10.1002/anie.201782761, 2017.
- Zhong, J., Kumar, M., Francisco, J. S., and Zeng, X. C.: Insight into chemistry on cloud/aerosol water surfaces, *Acc. Chem. Res.*, 51, 1229-1237, 2018.
- Zhong, J., Li, H., Kumar, M., Liu, J., Liu, L., Zhang, X., Zeng, X. C., and Francisco, J. S.: Mechanistic
815 Insight into the Reaction of Organic Acids with SO₃ at the Air-Water Interface, *Angew. Chem. Int. Ed.*, 131, 8439-8443, 2019.
- Zhong, J., Zhao, Y., Li, L., Li, H., Francisco, J. S., and Zeng, X. C.: Interaction of the NH₂ Radical with the Surface of a Water Droplet, *J. Am. Chem. Soc.*, 137, 12070-12078, 10.1021/jacs.5b07354, 2015.
- Zhong, J., Zhu, C., Li, L., Richmond, G. L., Francisco, J. S., and Zeng, X. C.: Interaction of SO₂ with the
820 Surface of a Water Nanodroplet, *J. Am. Chem. Soc.*, 139, 17168-17174, 2017.
- Zhu, C., Kumar, M., Zhong, J., Li, L., Francisco, J. S., and Zeng, X. C.: New Mechanistic Pathways for Criegee-Water Chemistry at the Air/Water Interface, *J. Am. Chem. Soc.*, 138, 11164-11169, 10.1021/jacs.6b04338, 2016.
- Zhu, C., Kais, S., Zeng, X. C., Francisco, J. S., and Gladich, I.: Interfaces select specific stereochemical
825 conformations: the isomerization of glyoxal at the liquid water interface, *J. Am. Chem. Soc.*, 139, 27-30, 2017.
- Zhuang, Y., and Pavlish, J. H.: Fate of hazardous air pollutants in oxygen-fired coal combustion with different flue gas recycling, *Environ. Sci. Technol.*, 46, 4657-4665, 2012.

Table 1. The rate constant ($\text{cm}^3 \cdot \text{molecule}^{-1} \cdot \text{s}^{-1}$) for the $\text{SO}_3 + \text{H}_2\text{SO}_4$ reaction and the effective rate constant ($\text{cm}^3 \cdot \text{molecule}^{-1} \cdot \text{s}^{-1}$) for the $\text{SO}_3 + \text{H}_2\text{SO}_4$ reaction with H_2O (100%RH) within the temperature range of 280-320 K

$T/(\text{K})$	280 K	290 K	298 K	300 K	310 K	320 K
k_{DSA}	5.52×10^{-12}	4.60×10^{-12}	3.95×10^{-12}	3.80×10^{-12}	3.13×10^{-12}	2.57×10^{-12}
$k'_{\text{DSA_WM_o}}$	2.12×10^{-13}	2.68×10^{-13}	2.88×10^{-13}	2.89×10^{-13}	2.89×10^{-13}	2.75×10^{-13}
$k'_{\text{DSA_WM_s}}$	1.03×10^{-11}	8.55×10^{-12}	7.42×10^{-12}	7.11×10^{-12}	5.79×10^{-12}	4.60×10^{-12}

k_{DSA} is the rate constant for the $\text{SO}_3 + \text{H}_2\text{SO}_4$ reaction; $k'_{\text{DSA_WM_o}}$ and $k'_{\text{DSA_WM_s}}$ are respectively the effective rate constants for H_2O -assisted $\text{SO}_3 + \text{H}_2\text{SO}_4$ reaction occurring through one-step and stepwise routes.

Table 2. The rate ratio between the $\text{SO}_3 + \text{H}_2\text{SO}_4$ reaction and the hydrolysis of SO_3 at different altitudes in the atmosphere of Venus

H (km)	T(K)	P (Torr)	$[\text{H}_2\text{O}]$	$[\text{H}_2\text{SO}_4]$	k_{DSA}	$k_{\text{DSA_WM_s}}$	$k_{\text{SA_WM}}$	$\nu_{\text{DSA}}/\nu_{\text{SA}}$
40	410	2025	1.08×10^{15}	6.15×10^{13}	5.22×10^{-12}	1.43×10^{-12}	2.31×10^{-13}	3.24×10^8
50	340	750	5.17×10^{14}	1.23×10^{14}	1.12×10^{-12}	3.87×10^{-12}	5.43×10^{-13}	3.81×10^{10}
60	320	104	1.72×10^{14}	1.85×10^{14}	1.23×10^{-12}	7.80×10^{-12}	1.37×10^{-12}	5.12×10^{10}
70	270	19	8.61×10^{13}	8.61×10^{13}	1.07×10^{-12}	8.61×10^{-12}	1.82×10^{-12}	5.23×10^{10}

k_{DSA} , $k_{\text{DSA_WM_s}}$ and $k_{\text{SA_SA}}$ are respectively the rate constants for $\text{SO}_3 + \text{H}_2\text{SO}_4$ reaction, H_2O -assisted $\text{SO}_3 + \text{H}_2\text{SO}_4$ reaction occurring through stepwise route and the hydrolysis reaction of $\text{SO}_3 + (\text{H}_2\text{O})_2$.

Table 3. Gibbs free energy (ΔG , kcal·mol⁻¹) for the formation of S₂O₇²⁻···H₂SO₄, S₂O₇²⁻···HNO₃, S₂O₇²⁻···(COOH)₂, H₃O⁺···NH₃, H₃O⁺···H₂SO₄, HSO₄⁻···H₂SO₄, HSO₄⁻···(COOH)₂, HSO₄⁻···HNO₃, H₂SO₄···NH₃, SO₇²⁻···H₂SO₄···NH₃, HOOCCH₂COOH···H₂SO₄···NH₃, HOCCOOSO₃H···H₂SO₄···NH₃, CH₃OSO₃H···H₂SO₄···NH₃ and HOOCCH₂CH(NH₂)COOH···H₂SO₄···NH₃ at 298 K

	S ₂ O ₇ ²⁻ ···H ₂ SO ₄	S ₂ O ₇ ²⁻ ···HNO ₃	S ₂ O ₇ ²⁻ ···(COOH) ₂	H ₃ O ⁺ ···NH ₃	H ₂ SO ₄ ···NH ₃
ΔG	-46.3	-30.6	-39.9	-51.7 (-49.2) ^a	-8.9 (-8.9) ^a
	H ₃ O ⁺ ···H ₂ SO ₄	HSO ₄ ⁻ ···H ₂ SO ₄	HSO ₄ ⁻ ···(COOH) ₂	HSO ₄ ⁻ ···HNO ₃	S ₂ O ₇ ²⁻ ···H ₂ SO ₄ ···NH ₃
ΔG	-27.5 (-27.0) ^a	-41.6	-33.6	-27.8	-40.1
	HOOCCH ₂ COOH ···H ₂ SO ₄ ···NH ₃	HOCCOOSO ₃ H ···H ₂ SO ₄ ···NH ₃	CH ₃ OSO ₃ H ···H ₂ SO ₄ ···NH ₃	HOOCCH ₂ CH(NH ₂)COOH ···H ₂ SO ₄ ···NH ₃	HOCH ₂ COOH ···H ₂ SO ₄ ···NH ₃
ΔG	-13.1 (-13.6) ^b	-20.4 (-22.5) ^c	-18.8 (-20.7) ^d	-13.2 (-14.0) ^e	-12.8 (-13.5) ^f

Energies are given in kcal·mol⁻¹, and calculated at the M06-2X/6-311++G(2df,2pd) theoretical level. References are as follows: [a] Zhong et al., 2019.; [b] Zhang et al., 2018.; [c] Rong et al., 2020.; [d] Gao et al., 2023.; [e] Liu et al., 2021a; [f] Zhang et al., 2017.

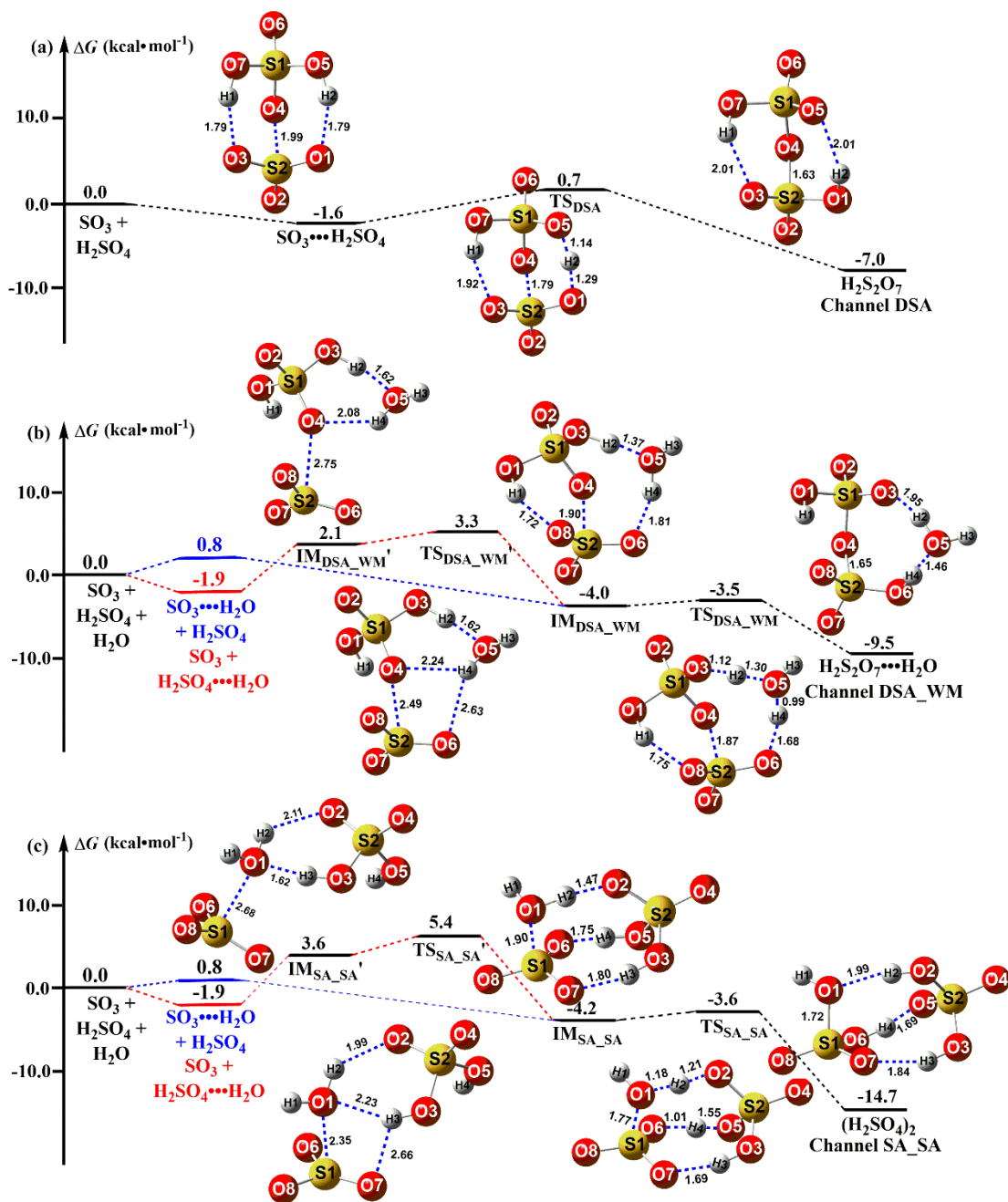


Figure 1. Schematic potential energy surface for the $\text{SO}_3 + \text{H}_2\text{SO}_4 \rightarrow \text{H}_2\text{S}_2\text{O}_7$ reaction; Distances is in angstrom at the M06-2X/6-311++G(2df,2pd) level, while the energy values correspond to the calculations at the CCSD(T)-F12/cc-pVDZ-F12//M06-2X/6-311++G(2df,2pd) level. The pre-reactive complex and TS for the route of DSA formation from the $\text{SO}_3 + \text{H}_2\text{SO}_4$ reaction with H_2O was denoted by “ $\text{IM}_{\text{DSA_WM}}$ ” and “ $\text{TS}_{\text{DSA_WM}}$ ”, respectively, while the corresponding pre-reactive complex and TS for the process of SA formation from the hydrolysis of SO_3 with H_2SO_4 was respectively labeled as “ $\text{IM}_{\text{SA_SA}}$ ” and “ $\text{TS}_{\text{SA_SA}}$ ”.

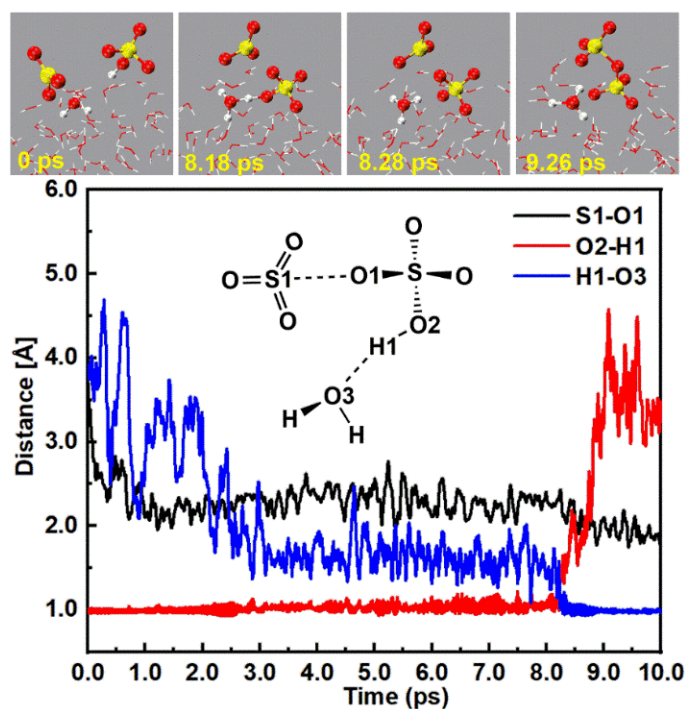


Figure 2. Top panel: Snapshot structures taken from the BOMD simulations, which illustrate H₂O-induced the formation of S₂O₇²⁻⋯H₃O⁺ ion pair from the reaction of SO₃ with HSO₄⁻ at the air-water interface. Lower panel: time evolution of key bond distances (S-O1, O2-H1, and O3-H1) involved in the induced mechanism.

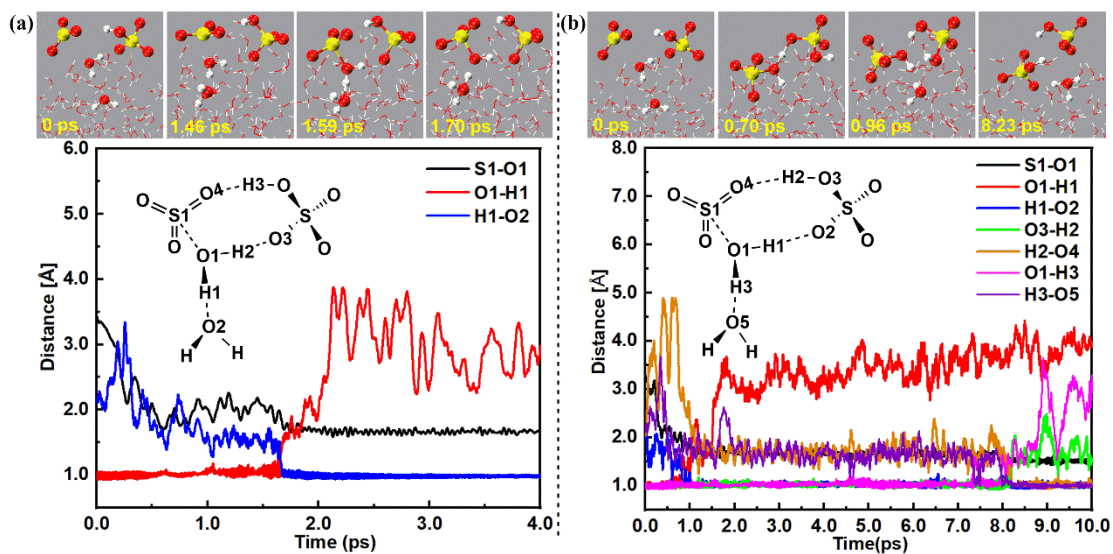


Figure 3. Top panel: Snapshot structures taken from the BOMD simulations, which illustrate the hydration reaction mechanism of SO_3 mediated by HSO_4^- at the air water interface. Lower panel: time evolution of key bond distances (S-O1, O1-H2, O5-H2, O2-H1, O3-H4 and O4-H3) involved in the hydration mechanism.

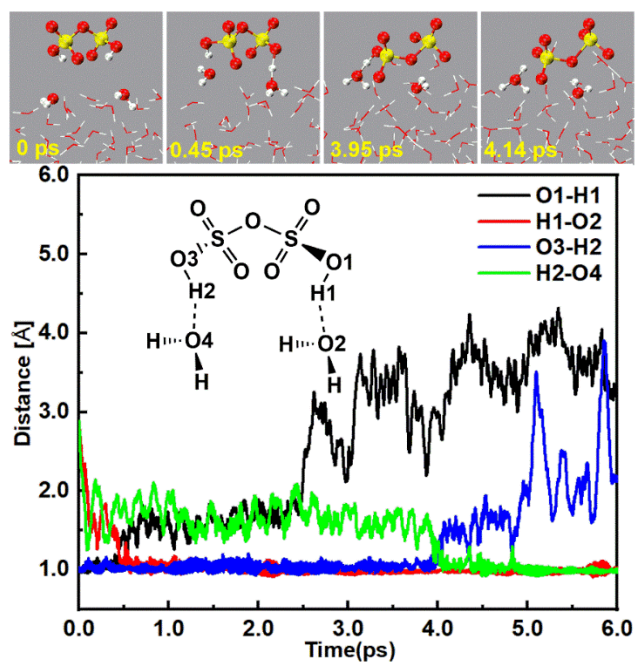


Figure 4. Top panel: Snapshot structures taken from the BOMD simulations, which illustrate the deprotonation of $\text{H}_2\text{S}_2\text{O}_7$ at the air water interface. Lower panel: time evolution of key bond distances (O1-H1, O1-H2, O3-H2 and H2-O4) involved in the hydration mechanism.

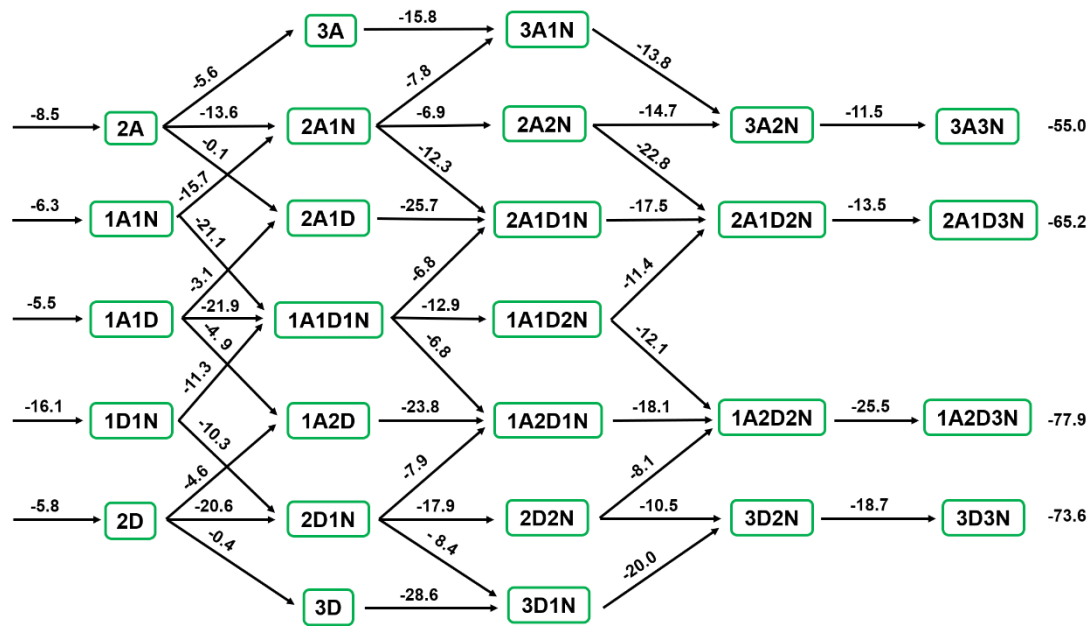


Figure 5. The Gibbs free energy (kcal·mol⁻¹) diagram of (DSA)_x(SA)_y(A)_z ($z \leq x + y \leq 3$) clusters at 278.15K and 1 atm. “A” refers to sulfuric acid, “D” refers to disulfuric acid and “N” refers to ammonia.

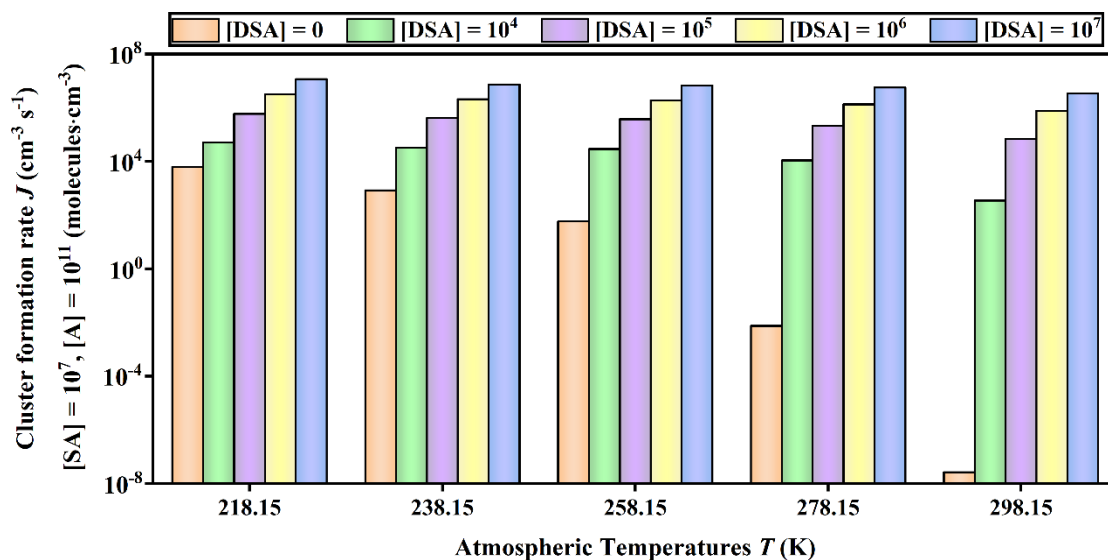


Figure 6. Cluster formation rates J ($\text{cm}^{-3} \text{s}^{-1}$) against the of DSA monomer concentration (unit: $\text{molecules}\cdot\text{cm}^{-3}$) under different temperatures (218.15, 238.15, 258.15, 278.15 and 298.15 K) where $[SA] = 10^7 \text{ molecules}\cdot\text{cm}^{-3}$ and $[A] = 10^9 \text{ molecules}\cdot\text{cm}^{-3}$.

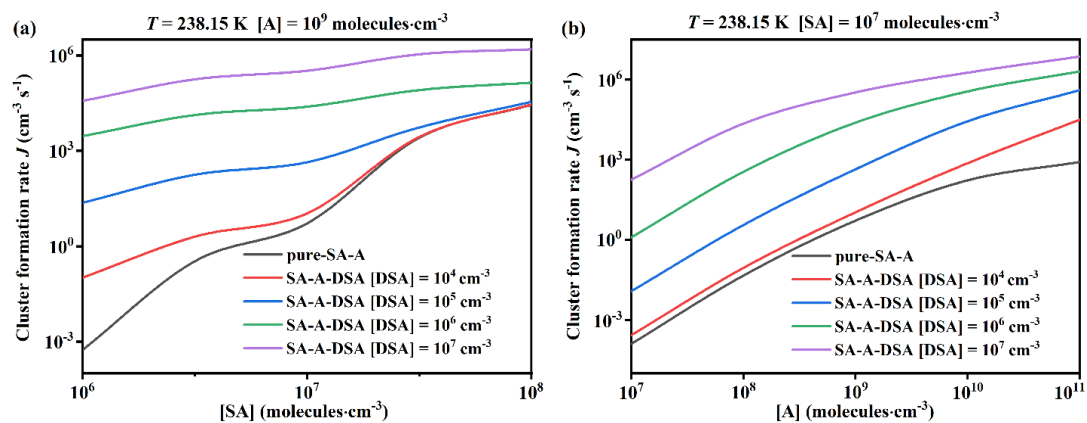


Figure 7. Simulated cluster formation rates J ($\text{cm}^3 \text{s}^{-1}$) as a function of (a) $[\text{SA}]$, (b) $[\text{A}]$, with different concentrations of disulfuric acid $[\text{DSA}]$ of 10^4 (red), 10^5 (blue), 10^6 (green), 10^7 (purple) and 0 molecules· cm^{-3} (black, pure-SA-A), at $T = 238.15 \text{ K}$.

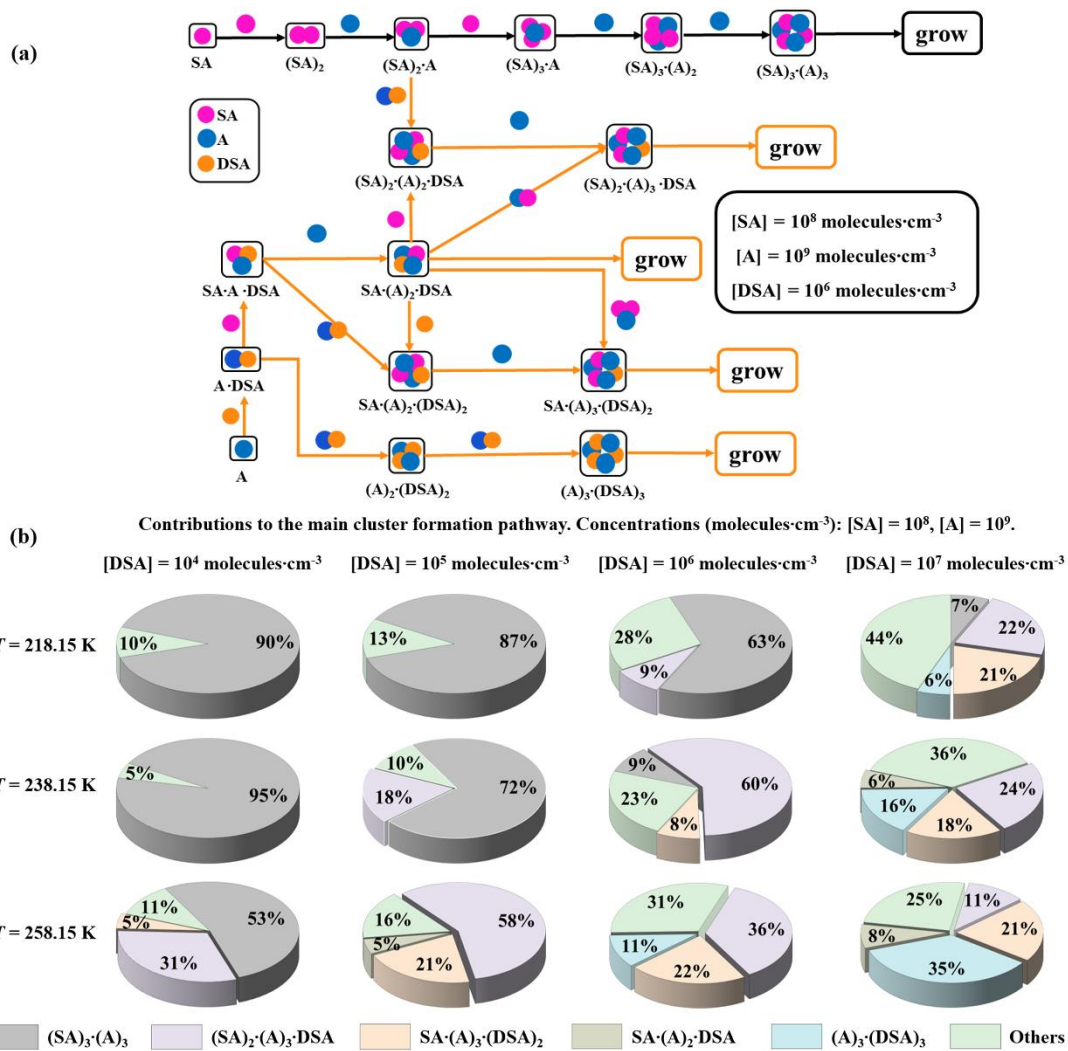


Figure 8. (a) The main pathways of clusters growing out of the research system under the conditions where 218.15 K, 238.15 K and 258.15 K, [SA] = 10⁸ molecules·cm⁻³, [A] = 10⁹ molecules·cm⁻³, and [DSA] = 10⁶ molecules·cm⁻³; (b) The contribution of different concentrations of DSA to the main cluster formation pathway at 218.15 K, 238.15 K and 258.15 K is shown in the pie charts.